Fall 2016

Understanding the uptake of polystyrene nanoparticles by the nasal mucosa

Ammar Sahib Abdulameer Al Khafaji
University of Iowa

UNDERSTANDING THE UPTAKE OF POLYSTYRENE NANOPARTICLES BY THE NASAL MUCOSA

by

Ammar Sahib Abdulameer Al Khafaji

A thesis submitted in partial fulfillment
of the requirements for the Master of
Science degree in Pharmacy
in the Graduate College of
The University of Iowa

December 2016

Thesis Supervisor: Professor Maureen D. Donovan

Graduate College
The University of Iowa
Iowa City, Iowa

CERTIFICATE OF APPROVAL

_____

MASTER'S THESIS

_____

This is to certify that the Master's thesis of

Ammar Sahib Abdulameer Al Khafaji
has been approved by the Examining Committee for
the thesis requirement for the Master of Science degree
in Pharmacy at the December 2016 graduation.

Thesis Committee: _____
Maureen Donovan, Thesis Supervisor

_____
Dale Wurster

_____
Aliasger Salem

_____
Lewis Stevens

_____
Ramprakash Govindarajan

With Love,
to my family and my friends.

ACKNOWLEDGEMENTS

I would like to thank my advisor, Professor Maureen D. Donovan for her guidance, support, and immense knowledge. I will forever be humbled by her scientific and professional approach and valuable experience.

I thank Dr. Wurster, Dr. Salem, Dr. Stevens, and Dr. Ramprakash for serving as Committee members, and for their critical evaluation and guidance. I extend my gratitude to all of the faculty members and students of Pharmaceutics and Translational Therapeutics (PTT).

ABSTRACT

Intranasal drug delivery is a very attractive pathway for administering drugs because of its ease of administration, the rapid absorption of most molecules, the ability to provide both local and systemic drug effects, the avoidance of the harsh gastrointestinal environment and first-pass hepatic metabolism, and the potential to deliver drugs directly to the brain. Nanoparticles, in some cases, may provide superior nasal drug delivery systems compared to administering the free drug alone. Endocytosis is the main uptake pathway by which nanoparticles pass through the nasal mucosa, and endocytic pathways that are well-known to contribute to uptakes processes include clathrin-mediated endocytosis, macropinocytosis, and caveolae-mediated endocytosis. While the endo-lysosomal pathways of particles following clathrin-mediated endocytosis and macropinocytosis may result in additional drug delivery challenges, transcytosis can be accomplished with caveolae-mediated endocytosis.

The objectives of this study were to characterize the endocytic pathways involved in the uptake of commercially-produced, fluorescently-labelled, carboxylate-modified, 40 nm polystyrene nanoparticles across the nasal mucosa and to evaluate the contribution of each of the major endocytic pathways in the uptake process. The uptake of the nanoparticles was investigated in the nasal olfactory and respiratory mucosa and inhibition of specific endocytic pathways was accomplished by the inclusion of a variety of different pharmacologic inhibitors. Chlorpromazine, amiloride, and methyl-ß-cyclodextrin were each evaluated separately to investigate clathrin-mediated endocytosis, macropinocytosis, and caveolae-mediated endocytosis, respectively. Trypsin-EDTA was used to separate the epithelial cell layer from the underlying submucosa, and the concentration of nanoparticles in the epithelial layer and the submucosal layer was measured to evaluate the mucosal distribution of nanoparticles following nasal absorption.

While the nanoparticles were found to be translocated through the nasal olfactory epithelium primarily via caveolae-mediated endocytosis, all of the endocytic pathways were found to be significantly involved in the uptake of the particles by the respiratory epithelium following incubation for 30 min with nanoparticles. After a 60 min incubation, the activity of three endocytic pathways in both the nasal respiratory and olfactory tissues was apparent.

The overall mass of nanoparticles in the epithelial layer was found to be higher than in the submucosal layer in both tissue types. Moreover, the amount of nanoparticles that reached the submucosal tissues was found to be similar regardless of inhibition or tissue type. Finally, the endocytic activity of the nasal olfactory tissues was found to be approximately 2-fold higher than that of the nasal respiratory tissues.

PUBLIC ABSTRACT

Nanoparticles have many proposed advantages for use in nasal drug delivery systems. Nanoparticles can improve uptake and efficacy and lower toxicity compared to the drug alone. In order to study the transport behavior of nanoparticles across nasal tissues, the uptake of non-biodegradable, fluorescently-labeled, carboxylate-modified polystyrene nanoparticles was measured. These 40 nm particles are spherical in shape and loaded with fluorescein, a fluorescent dye that can be measured spectrophotometrically, to determine the number of particles that entered the nasal tissues. In order to identify the pathways involved in the uptake of these particles, a variety of pharmacologic inhibitors were also included in the nanoparticle transport studies. The results indicate that the nanoparticles enter the nasal tissues using several endocytic mechanisms, namely, macropinocytosis, clathrin-mediated endocytosis, and caveolin-mediated endocytosis. These findings suggest that more than one endocytic pathway is involved in the uptake process in the nasal tissues, and these multiple pathways may help to increase the total nanoparticle uptake in the nasal tissues.

TABLE OF CONTENTS

LIST OF TABLES

LIST OF FIGURES

CHAPTER I

INTRODUCTION

Intranasal Delivery Route

The nasal delivery route is an accessible drug delivery pathway which provides a relatively large surface area for absorption [1]. Intranasal administration has the possibility to deliver drugs both locally and systemically [2]. Local delivery allows for lower systemic drug exposure due to typically lower administered doses. Hence, side effects will be less frequently encountered. On the other hand, systemic absorption is possible when systemic therapy is intended due to the high vascularity of the nasal mucosa. Systemic intranasal delivery offers many advantages including: rapid absorption, avoiding the harsh environment of the gastrointestinal tract and limiting metabolism, especially avoiding hepatic, first-pass metabolism. Other advantages of the nasal delivery route include the convenient of self-administration and the potential for enhanced delivery to the brain [3].

Nasal Anatomy and Function

The nose is a complex organ that is designed to serve multi-physiologic functions. The main functions of the nasal cavity are as an air-passage to the lung, air cleansing, air humidification, and olfaction. The nasal cavity is composed of an approximately 5-cm high and 10-cm long dual chamber separated by the nasal septum [2]. The nasal chambers possess a total surface area of 150 cm^2 and their total volume is about 15 ml. The three main functional areas of the nasal cavity include the vestibular, respiratory, and olfactory regions [2] [Figure 1.1].

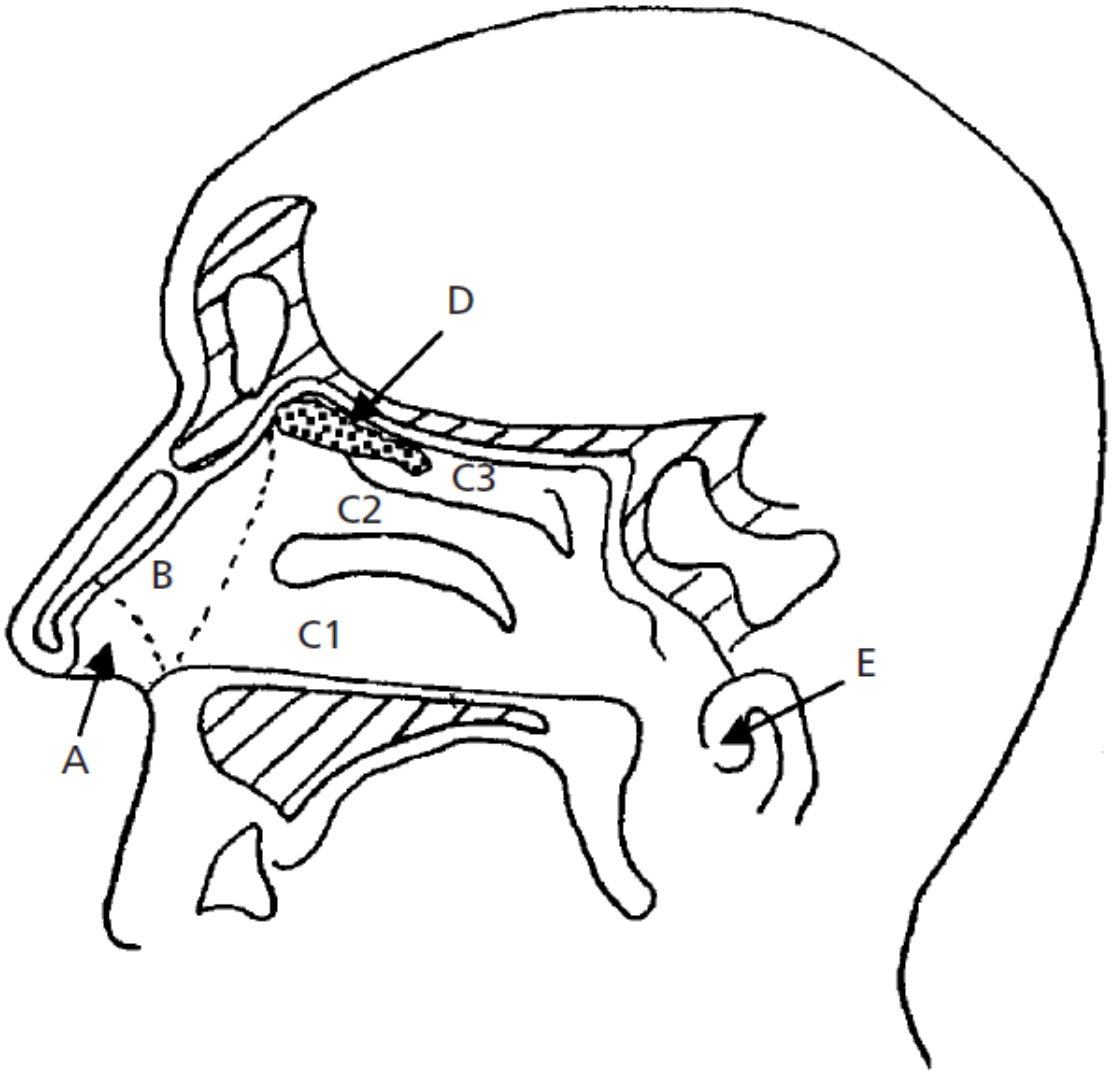

Figure 1.1. Sagittal section of the nasal cavity [4]. Abbreviations are: nasal vestibule (A), atrium (B), the respiratory region inferior turbinate (C1), middle turbinate (C2), and superior turbinate (C3), the olfactory region (D), and nasopharynx (E). Reproduced with permission.

Nasal Vestibular Region

The vestibular area contains approximately 0.6 cm^2 of the nasal cavity in humans. It is the entry way to the nasal cavity that precedes the nasal valve, a region which accounts for about 50% of the total resistance of the air flow between the nostril to the alveoli [5]. The epithelial layer of this region is composed of stratified squamous and keratinized epithelia with nasal hairs [2]. The vestibular region has low vascularization [2]. Due to its small surface area and low blood supply, this region is of limited interest in drug delivery to the nasal cavity.

Nasal Respiratory Mucosa

The respiratory region forms about 130 cm^2 of the total nasal cavity area in humans [2]. This region acts as an air-filtering and conditioning system. The respiratory mucosa (epithelium and submucosa) overlies three turbinates (inferior, middle, and superior) protruding from the lateral wall. The turbinates' shapes assist in temperature regulation and humidification of the inspired air by forcing the inhaled air stream between and over the turbinate surfaces allowing heat and water exchange between the tissue surface and the air [5]. The nasal turbinates enlarge the surface area of the nasal respiratory mucosa, thereby allowing more surface area to humidify and clean the inspired air [2]. The epithelial layer of this region is composed of a ciliated, pseudostratified columnar epithelium containing three major cell types including: columnar ciliated cells, goblet cells, and basal cells [5] [Figure 1.2].

Each ciliated columnar cell is covered by about 300 microvilli (small-finger like expansions of the cytoplasmic membrane) on the apical surface that allow for an increased absorptive surface area [5]. All ciliated columnar cells are covered by about 100 motile cilia (hair-like protrusions) extending from their cell surface that are mainly responsible for mucus clearance from the nasal cavity [5, 6]. The main functions of the columnar cells are absorption and mucociliary clearance.

Goblet cells are responsible for secreting and maintaining the mucus layer in this region. The mucus layer serves as a barrier entrapping inhaled particles and preventing them from reaching the lower respiratory tract. The mucus is cleared by the movement of cilia toward the nasopharynx in a process called mucociliary clearance. On average, the clearance process through the nasal cavity takes approximately 20 min, but this time frame allows for significant interindividual variability [2]. Basal cells (progenitor cells) serve to replace the columnar cells or goblet cells.

The respiratory submucosa is located beneath the epithelial layer. It is highly vascularized and represents a good target for local and systemic drug delivery [2].

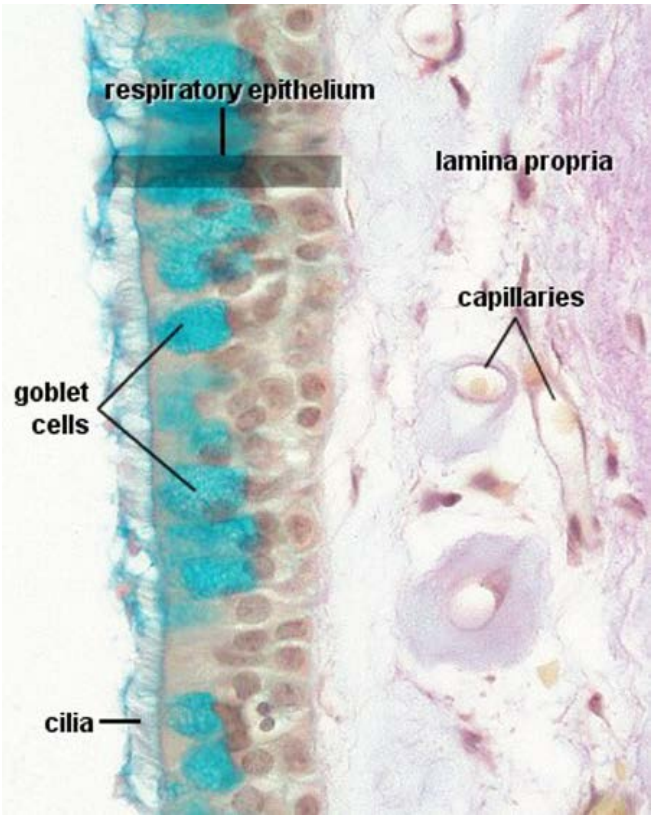

Figure 1.2. Histological section of the nasal respiratory mucosa [7].

Nasal Olfactory Mucosa

The olfactory mucosa (epithelium and submucosa) forms about 15 cm^2 of the total area of the nasal cavity in humans [2]. Its main function is olfaction (smelling). The olfactory region is situated in the superior region of the nasal cavity [Figure 1.1]. It is composed of a pseudostratified columnar epithelium with three main cell types: olfactory receptor cells, supporting cells, and basal cells [5] [Figure 1.3].

Olfactory receptor cells are bipolar neurons that are scattered among the supporting cells, and their nuclei are located near the middle of the epithelial layer [8]. Toward the apical epithelial surface, each olfactory cell extends its dendrite end which forms a knob-like structure containing about a dozen basal bodies from which cilia emerge to provide a considerable surface area for membrane chemoreceptors. These chemoreceptors generate action potentials following interactions with odoriferous materials which transmit signals along the axon that extends into the lamina propria. The axons of the olfactory receptor cells leave the epithelial layer and merge into small nerve bundles that reach the brain through the cribriform plate of the ethmoid bone and terminate in the olfactory bulb [8].

Supporting (sustentacular) cells are columnar epithelial cells that lie between the olfactory receptor cells in the olfactory epithelium. Their apical surfaces also contain microvilli but do not contain cilia [9]. The main functions of these cells are to provide physical support to the olfactory receptor cells, and to assist in maintaining a microenvironment essential for olfactory function and survival due to the abundant ion channels contained within these cells [8].

Basal cells are located at the base of the epithelial layer but do not reach the apical surface. They are small, spherical or cone-shaped stem cells providing a cell source for replacing olfactory

receptor cells or supporting cells that are lost during normal turnover or injury [9]. The submucosal region (lamina propria) is composed of a collagenous, dense, irregular connective tissue that is embedded with nerve bundles, Bowman's glands, and blood vessels [9]. The presence of the olfactory receptor cells makes the olfactory region a promising site for potential drug delivery to the brain.

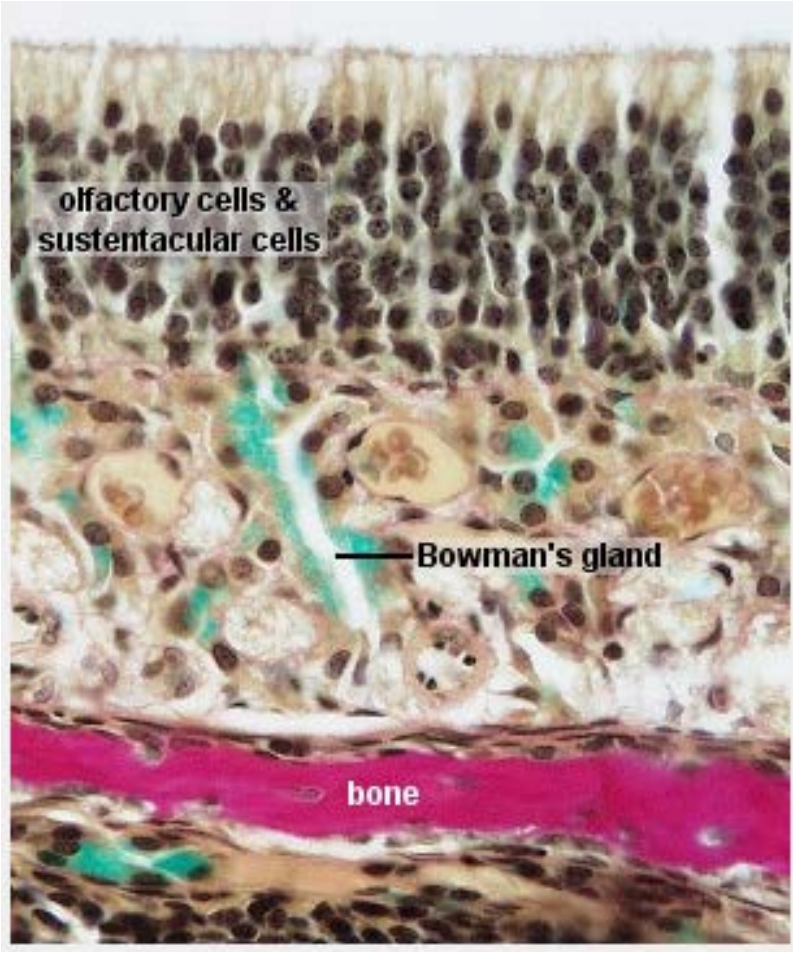

Figure 1.3. Histological section of the nasal olfactory mucosa [7].

Potential Pathways of Intranasal Drug and Nanoparticle Absorption

Upon contact with the nasal mucosa, molecules or particles can be absorbed across the nasal epithelium, resulting in potential local or systemic effects. In order for a compound to show a local effect or to reach the blood vessels in the submucosal region and then be transported to the systemic circulation, molecules or particles must first pass through the epithelial cells.

The passage of a compound through the nasal epithelium depends on two main factors: drug lipophilicity and molecular weight [10]. Relatively small molecules that are lipophilic tend to transfer across the lipophilic cell membrane by passive diffusion using a transcellular route. Passive diffusion is a non-active process that requires compound molecules to dissolve in the lipid bilayer and diffuse into the cytoplasm crossing to the opposite of the cell. Passive diffusion of molecules follows their concentration gradient across the cell membrane. Hydrophilic molecules, in comparison, might pass through the tight junctions between the cells if they are very small in size (less than ~ 300 Dalton) [10, 11]. Larger hydrophilic molecules may also be absorbed by the transcellular route, but their transport pathways are likely to involve either specific transporters such as organic cations (OCT) or amino acids transporters (AAT) or by endocytosis [Figure 1.4].

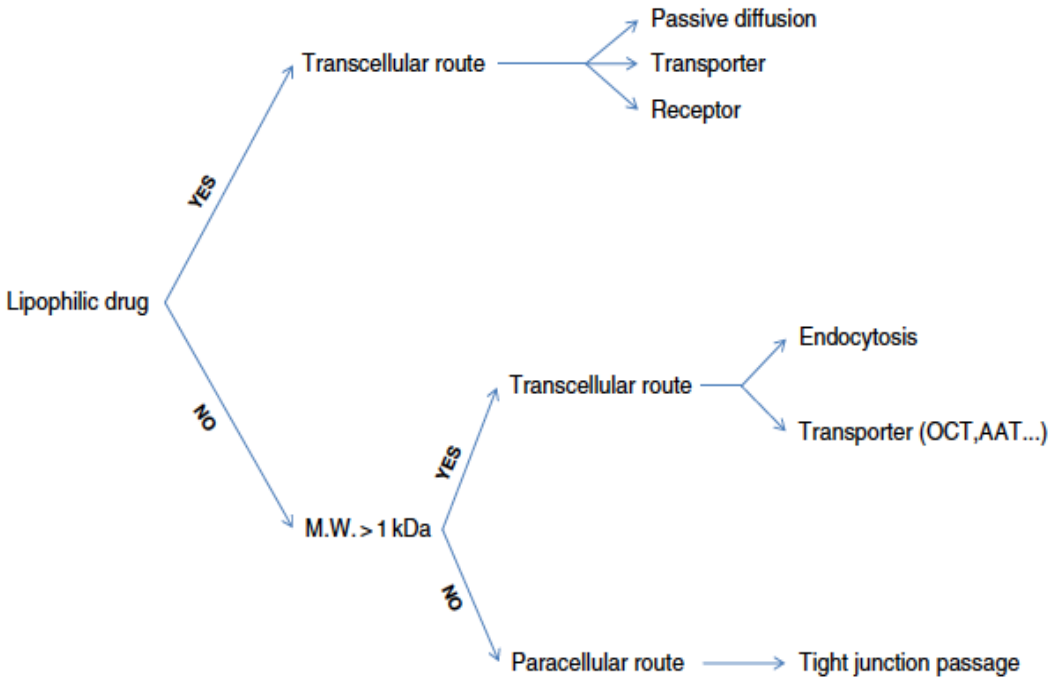

Figure 1.4. Possible mechanisms by which drug molecules cross the nasal epithelium depending on lipophilicity and molecular size of the molecules [11]. Abbreviations are: OCT: organic cations transporters, AAT: amino acids transporters. Reproduced with permission.

Nanoparticles as Nasal Delivery Systems

A nanoparticle is a solid particle with a size of less than 100 nm [12]. As nasal delivery systems, nanoparticles may improve uptake and efficacy and reduce toxicity compared to the free drug molecule due to small size and possible higher dose administration. For example, 130-nm albumin nanoparticles loaded with paclitaxel (Abraxane®) were approved by the U.S. Food and Drug Administration for intravenous cancer treatment. Administering the drug in a nanoparticle formulation offers many advantages such as improved efficacy due to a higher administered dose and reduced toxicity [13].

Mechanisms of Nanoparticle Uptake by the Nasal Tissues

Particles in the nano-size range likely cross cell membranes via endocytosis, a cellular uptake mechanism in which part of the cell membrane encloses around a particle and then separates from the membrane as a vesicle or vacuole carrying the particle into the intracellular matrix. The process of endocytosis involves three main steps; First, forming a vesicle or vacuole (endosome) from the cell membrane which engulfs the particle(s) in contact with the cell surface. Second, the endosome travels into the intracellular matrix where its cargo is sorted mainly based on the intra-endosomal acidity (pH-dependent sorting) and delivered to different regions of the intracellular compartment. Finally, the cargo will be further directed or processed within the cell, or recycled to the extracellular environment [14].

Endocytic processes are divided into two major categories: phagocytosis and pinocytosis [Figure 1.5]. Phagocytosis is the uptake of large particles by special phagocytic cells such as macrophages and dendritic cells [15]. Pinocytosis is the uptake of small particles and is a process that can happen in any cell. Pinocytosis is the main mechanism by which nanoparticles can be translocated through a cell membrane [14]. Pinocytosis can be divided into clathrin-mediated and clathrin-independent endocytic mechanisms based on the proteins involved in the formation of endosomes by a specific pinocytosis process [14].

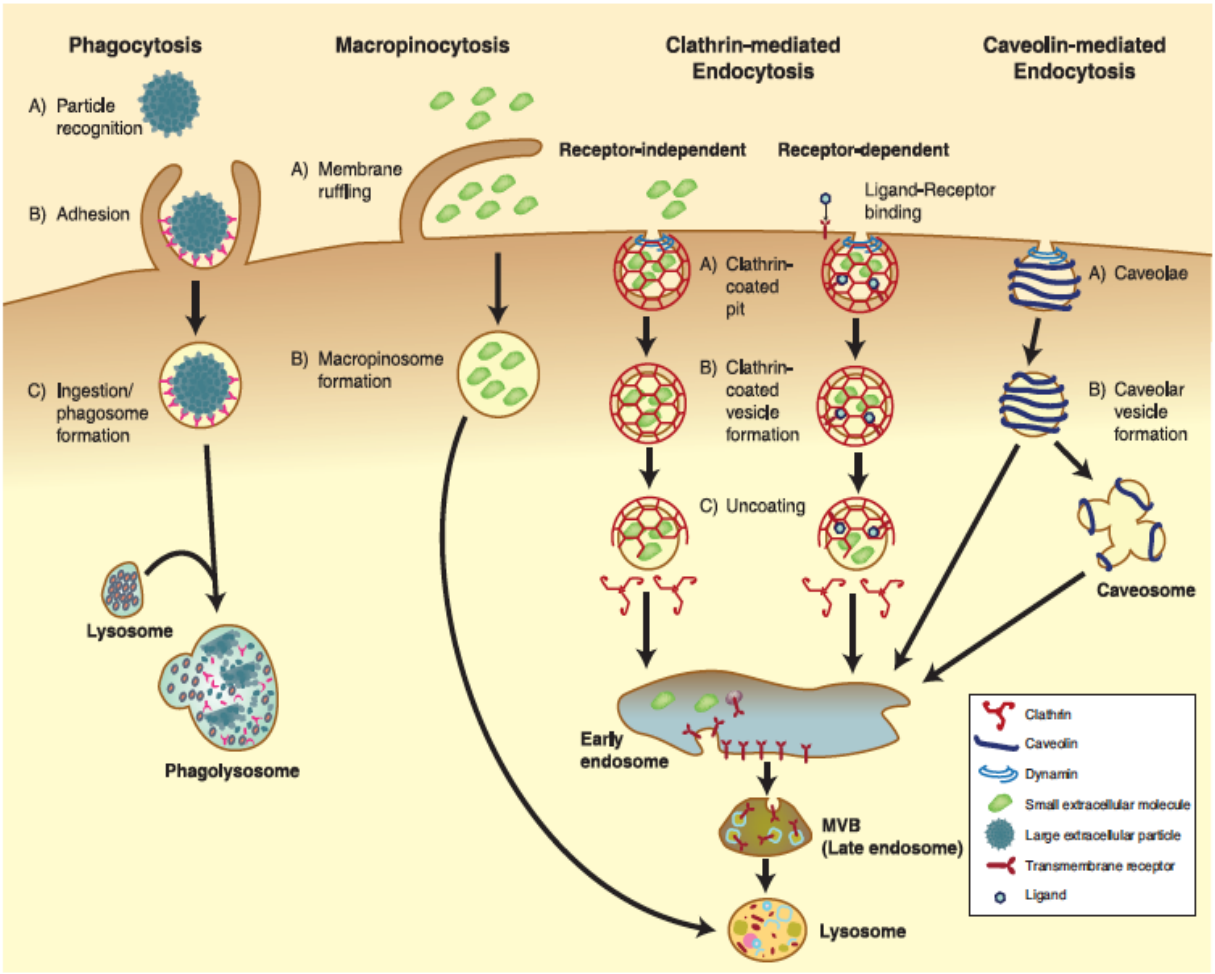

Figure 1.5. Examples of cellular endocytic pathways [16]. Phagocytosis only occurs in macrophages and dendritic cells. Other endocytic pathways take place in all cells. The initial step of endocytosis requires cargo uptake into intracellular vesicles. The second step is cargo sorting by endosomes. The final step is cargo delivery to its final intracellular destination or recycling to the extracellular environment (not shown). Abbreviation: MVB: multivesicular body. Reproduced with permission.

Clathrin-mediated endocytosis requires clathrin, an intracellular protein that assists in deforming the plasma membrane into a clathrin-coated vesicle. Clathrin-mediated endocytosis is responsible for the uptake of essential nutrients like cholesterol that arrives at the cell associated with low density lipoproteins (LDL) which interact with low density lipoprotein receptors (LDLR) on the cell membrane [14]. A clathrin coated vesicle has a size of about 120 nm [15]. Once the vesicle is released into the intracellular medium, the clathrin coat is shed by the action of the ATPase heat shock cognate 70 (HSC70) and its vesicle attached cofactor, auxilin, and the uncoated vesicle can be delivered to different compartments inside the cell, can fuse with lysosomes for final degradation, or can be transported to outside of the cell (transcytosis) [14, 17].

Clathrin-independent endocytosis does not require the clathrin coat protein and can be sub-classified as macropinocytosis, caveolae-mediated endocytosis, and caveolae and clathrin-independent endocytosis.

Macropinocytosis is a caveolae and clathrin-independent, actin-driven pathway of endocytosis [15]. This pathway is involved in the uptake of dead cells fragments, viruses, and bacteria. Macropinocytosis can form a vesicle within the size range of about 0.5-10 μm and can take up both nano and micro-size particles [14]. Macropinocytosis is initiated by transient activation of the tyrosine kinase receptor by growth factors [15]. Activation this receptor leads to actin polymerization, the formation of membrane ruffles and macropinosome formation [15]. Once the vesicle is separated from the cell membrane, macropinosomes fuse with lysosomes for final processing and degradation.

Caveolae-mediated endocytosis happens in all cells of the body except in neurons and leukocytes, due to the lack of the caveolin protein in these cells types [18]. This pathway might be involved in

protein endocytosis [15]. Caveolae originate from a region in the plasma membrane that is rich in cholesterol (lipid raft) to which caveolin, the main membrane integral protein that coats the caveolae, is attached [14]. Caveolae have a size range between 50-80 nm and their flask-shape is due to the presence of a caveolin protein coat [14, 19]. Upon releasing into the intracellular compartment, the caveolae deliver their content to either the Golgi apparatus or the endoplasmic reticulum for sorting and/or to the other side of the cell membrane (transcytosis) [15, 20]. The neutral pH of caveolae protect their cargos from degradation by avoiding the hydrolytic environment of lysosomes. Many bacterial toxins and cell surface proteins may enter the cell using this pathway [14, 15].

Caveolae- and clathrin-independent endocytosis are other pathways of pinocytosis in which clathrin and caveolin do not participate in endosome coating or formation. These pathways require further characterization since they have many subtypes, and few reports exist describing nanoparticles utilizing these pathways for their cell entry [14].

Perturbation of Endocytosis Using Pharmacologic Inhibitors

Since each endocytic pathway has specific characteristics and activation triggers, along with endosomal structural differences and fates, it is important to understand the contribution of each process in the uptake of nanoparticles. The physical and chemical characteristics of the particles are major factors that influence their uptake pathways. It has been reported that particles with negative surface charges trigger uptake by caveolae-mediated endocytosis, and the charge at the surface of the particles might also trigger other endocytic pathways [15]. There are a number of reports in the literature on the effect of the surface charge on the uptake of the particles, yet consensus regarding mechanisms has not been reached.

In order to further investigate the effects of particle characteristics on the uptake by each endocytic pathway and the contribution of each process in the total uptake, pharmacologic inhibitors of endocytosis have been included in transport studies to more readily evaluate the key uptake mechanisms.

Inhibition of clathrin-mediated endocytosis can be achieved by the use of hypertonic sucrose, potassium depletion, cytosolic acidification, and the antihistamine, chlorpromazine (CPZ) [21]. CPZ is a widely used cationic amphipathic drug that can inhibit clathrin-mediated endocytosis when used in micromolar concentrations [21]. CPZ is able to interfere with the attachment of the Adaptor Protein 2 (AP-2) to the plasma membrane [22]. AP-2 is an intracellular protein that is responsible for linking clathrin to the cell membrane, and, if this linking does not occur, clathrin is not recruited and vesicles do not form.

Macropinocytosis can be inhibited by the use F-actin-depolymerizing drugs, phosphoinositide metabolism inhibitors, and sodium-proton exchange (SPE) inhibitors [21]. SPE is essential in maintaining cytosolic pH and providing an optimal medium for actin polymerization in the immediate vicinity of the plasma membrane. Amiloride has been used extensively as an SPE inhibitor [21]. By lowering the submembranous pH, amiloride inhibits actin polymerization and blocks macropinocytosis [23].

Cholesterol is a critical membrane component for caveolae-mediated endocytosis. Traditionally, caveolae-mediated endocytosis has been inhibited by modifying the chemical properties or the content of cholesterol in the cell membrane. Statins, filipin, cholesterol oxidase, and cyclodextrins have been studied and utilized as a means for inhibiting caveolae-mediated endocytosis [21]. Methyl-β-cyclodextrin (m-βCD) has been widely used to extract cholesterol from the plasma

membrane [21, 24-26]. M-βCD is a cyclic heptasaccharide with a hydrophobic core that is able to form a soluble inclusion complex with cholesterol, thereby lowering its content in the membrane. Without cholesterol, the resulting caveolae will be flattened and the carrying capacity of the vesicle is negatively impacted [26].

Specific inhibition of caveolae and clathrin-independent endocytosis has not been effectively accomplished due to the difficulty in characterizing the mechanism of vesicle formation for these pathways.

Hypothesis and Specific Aims

Nanoparticles provide a great opportunity for drug delivery; they provide several advantages such as potential uptake and efficacy improvements for drug compounds with low permeabilities and reduced systemic toxicity compared to the drug alone. However, the transport mechanisms involved in nanoparticle uptake across biological barriers are not fully understood. In particular, identifying and optimizing uptake and distribution for improved effect is difficult in the absence of this knowledge. Understanding the uptake mechanisms of nanoparticles in the nasal mucosa could help to predict their transport behaviors and improve their utility for both local and systemic therapies.

Many endocytic pathways are involved in the uptake of nanoparticles by the nasal tissues. However, in most cases only one or two routes play a significant role in the uptake process [27]. Endocytic pathways that are involved in translocating nanoparticles within the nasal respiratory mucosa may be different in their contribution from those of the nasal olfactory mucosa, i.e. different nasal cell types show different endocytic activities. The uptake of 20 nm, carboxylate-modified, polystyrene nanoparticles (CM-PNPs) by the nasal respiratory mucosa was shown to occur mainly through clathrin-mediated endocytosis while no specific endocytic pathway was shown to be significantly involved in the uptake by the nasal olfactory mucosa [27]. In comparison, the uptake of 100 nm CM-PNPs by the nasal respiratory mucosa was shown to be mediated mainly by macropinocytosis and caveolae-mediated endocytosis. However, macropinocytosis was the only pathway significantly involved in the translocation of these relatively large nanoparticles by the nasal olfactory mucosa [27].

Targeting nanoparticles to a specific endocytic pathway can help to determine their ultimate fate inside the cell [14]. To understand and explore the effect of size on the uptake of nanoparticles by each specific endocytic route, the endocytic uptake pathways of 40 nm CM-PNPs (nano-size particles are within the size range of naturally occurring particles like LDL and LDLR) were investigated in excised nasal respiratory and olfactory mucosa.

The underlying hypothesis of this research is that several endocytic pathways are involved in the uptake of 40-60 nm CM-PNPs in the nasal mucosa, and the primary mechanisms differ between the nasal respiratory and olfactory epithelia.

To test our hypothesis, we will address the following specific aims:

1. Determine the overall uptake of 40 nm fluorescently-labeled CM-PNPs in excised nasal respiratory and olfactory tissues using NaviCyte® diffusion cells.
2. Compare the effects of known pharmacologic inhibitors on 40 nm CM-PNP uptake in the nasal respiratory and olfactory mucosa.

CHAPTER II

EXPERIMENTAL PROCEDURE

Materials and Instrumentation

Polystyrene latex nanoparticles (40nm FluoSpheres® YG, CM-PNPs) were obtained from Life Technologies, Inc. (Eugene, OR). These yellow-green, fluorescent nanoparticles are uniform, polystyrene nanospheres with excitation and emission wavelengths for detection of 505 nm and 515 nm, respectively [28]. Particles were supplied as an azide free suspension (5% w/v) in distilled water in 1mL vials. The fluorescence emitted from the FluoSpheres® YG particles is produced by fluorescein loaded into the particles. 2-Ethoxyethyl acetate (Cellosolve® acetate) was purchased from Alfa Aesar Co. (Sparks, NV). The preparation of Krebs Ringer Bicarbonate buffer (KRB) is described in Appendix A. A SpectraMax M5 Multi-Mode Microplate Reader (Molecular Devices, Sunnyvale, CA) using a 96 well quartz plate was used for measuring fluorescence intensity in all studies. An AccuSpin ™ 400 centrifuge (Fisher Scientific) to centrifuge samples were used throughout the experiments. A FS20 ultrasonicator was used for samples' sonication. A Malvern Zetasizer Nano-ZS was used to measure zeta potentials and the particle sizes of the commercial nanoparticles. An EVOM2 (World Precision Instruments) was used to measure the transepithelial electrical resistance (TEER). A CORNING Pinnacle 545 pH meter was used for pH measurement.

Sample Preparation for Particle Size and Zeta Potential Determination

The commercial nanoparticle suspension (5% w/v, Invitrogen) was diluted with either Nanopure water or KRB to reach a final concentration of 0.002% w/v [27]. These prepared suspensions were vortexed and sonicated for 4 minutes to disperse the nanoparticles and degas the sample. Finally,

the suspension was cooled to room temperature before conducting particle size or zeta potential measurements.

Particle Size Measurement

A sample of 1mL of the prepared suspension (0.002% w/v) [27] was withdrawn and transferred to a plastic cuvette (Fisherbrand™ Disposable Cuvettes, 1.5 mL) to measure the size of the particles. The sample was equilibrated in the instrument for 60 seconds, and the measurement was conducted at 24.5^{o} C using a Malvern Zetasizer Nano-ZS.

Zeta Potential Measurement

A sample of 1mL of the prepared suspension (0.002%) [27] was withdrawn and transferred to a folded capillary cell (Malvern, Worcestershire, UK) to measure the zeta potential of the particles. The sample was equilibrated for 60 seconds, and the measurement was conducted at 24.5^{o} C using a Malvern Zetasizer Nano-ZS.

Transport Experimental Methods

Transport studies were carried out in two different media. First, we evaluated the uptake of nanoparticles in olfactory and respiratory nasal tissues in KRB. Second, we incorporated pharmacological inhibitors of endocytosis in different transport media in order to examine the contribution of each endocytic pathway in the uptake process. Then, we compared the results from the pharmacologically-inhibited tissues to the untreated media tissues to understand the importance of each endocytic pathway. In all of these studies, the amount of nanoparticles in the epithelial layer and the submucosal layer were measured to understand the distribution of nanoparticles within the nasal mucosal tissues.

Dye Extraction Using Cellosolve® Acetate

Since nasal tissues are considered to be low density tissues, no preliminary digestion step is required to extract the dye, fluorescein, from these tissues [29]. The extraction procedure for the dye can be performed by directly immersing the tissue in an organic solvent to dissolve the nanospheres and release the dye into the solvent medium to be subsequently measured by a spectrofluorimeter. 2-ethoxyethyl acetate (Cellosolve® acetate) was chosen as a solvent for the extraction procedure [30]. This organic solvent has the ability to dissolve polystyrene and has a low volatility so that solvent loss is reduced and personal toxicity from inhalation is decreased. Cellosolve® acetate is a clear liquid which is immiscible with water at room temperature. In order to extract the dye completely from the nasal tissue explants, samples were incubated with 3mL Cellosolve® acetate for 48 hour [30] at 37° C in the dark [27]. This allows the nanospheres to dissolve and release the dye into the solvent medium. Once the dye is in the solvent phase, its fluorescence intensity can be measured using a spectrofluorimeter.

Preparation of Bovine Olfactory and Respiratory Mucosa

Bovine nasal mucosa, which is a useful model for human nasal mucosal specimens [31, 32], was used as an *in vitro* model to investigate the transport of nanoparticles through the nasal tissues. Fresh bovine nasal mucosae were obtained from Bud's Custom Meats Co., Riverside, IA. Nasal olfactory and respiratory mucosae were excised from the nasal cavities of freshly killed cows. The olfactory and respiratory mucosae were exposed by making incisions along the lateral walls of the nasal cavity and a horizontal incision was made along the ocular plane [27, 31, 33]. The nasal tissues were harvested carefully and stored in KRB on ice during transport to the laboratory within a period of no more than 20 min.

Standard Curve Determination

It has been shown that it is possible to quantify polystyrene latex beads by measuring the fluorescence intensity of the dye within the beads [29]. The relationship of the dye concentration inside the particles (particle loading) with the fluorescence intensity was determined by incubating the particles with Cellosolve® acetate solution in the dark for 48 hours.

To construct a standard curve, fractions (10 µL, 5 µL, 2.5 µL, 1.25 µL, 0.625 µL) of diluted nanosphere stock suspensions (0.1% w/v) were withdrawn and combined with 10 ml Cellosolve® acetate in 15 mL polypropylene tubes [27, 34]. After sealing with Parafilm®, these solutions were incubated for 48 hours in the dark at 37° C with shaking (VWR Incubating Orbital Shaker). After incubation, the relative fluorescence intensity of aliquots (100 µL) was measured by a SpectraMax M5 Multi-Mode Microplate Reader (Molecular Devices, Sunnyvale, CA) with a 96 well plate attachment [27]. A linear correlation between the dye fluorescence intensity and the particle concentration was found and used to determine the concentration of nanoparticles per mL of solvent in the transport experiments.

Cellosolve® Acetate Effect on Nasal Blank Olfactory and Respiratory Tissue

To examine the effect of the solvent on blank nasal mucosa tissues, excised olfactory or respiratory tissues were incubated with 3mL Cellosolve® acetate in 15 mL polypropylene tubes. After sealing with Parafilm®, the tubes were incubated for 48 hours in the dark at 37° C. After incubation, the samples were centrifuged and the fluorescence intensity of the supernatants were measured [27].

Transport Studies
Non-Inhibited Transport Studies

Transport studies were initiated within 10-15 minutes of returning to the laboratory following tissue harvesting. Small sections of the mucosa were stripped away from the cartilage using a small scissor or scalpel. The nasal tissues were affixed on the pins of NaviCyte® diffusion cells using a pair of tweezers, where the mucosal side of the tissue faced the donor chamber. To achieve stable electrophysiological measurements, the bovine tissues need to be equilibrated in the diffusion cells at 37º C for 20-30 minutes [27]. Since TEER provides a good indication of the viability of epithelial tissues [33], TEER measurements were used to assure the tissue integrity (Appendix C [Table C.10]).

Excised nasal tissues in NaviCyte® diffusion cells were equilibrated for 30 minutes at 37º C after placing KRB in both the donor and the receiver chambers. In order to retain tissue viability, the cell contents were circulated by gas lift (O_2/CO_2, 95% / 5%) at a rate of 1-2 bubbles per second [27, 33]. Following the equilibration time, the buffer was removed from the donor side and was replaced by 1mL of a nanoparticle-containing suspension at an initial concentration of 0.1% w/v prepared by diluting the commercially-obtained stock solution (5%) with fresh KRB. Immediately after replacing the donor side buffer, the buffer was removed from the receiver chamber and replaced with 1mL fresh KRB.

The transport studies were carried out at 37ºC for periods of 30 and 60 minutes. At the end of these studies, the tissues were removed from the NaviCyte® diffusion cells and were rinsed with fresh buffer solution to remove any free or loosely attached particles. After excision and weighing, the exposed sections of the tissues were subjected to further processing to quantify their nanoparticle

contents. Experiments were carried out in triplicate and were terminated after either 30 or 60 minutes of incubation with the nanoparticle suspension [27].

Epithelium Extraction and De-Epithelization

The excised nasal mucosal tissue is composed of two distinct layers: the upper epithelial layer and the lower submucosal layer. To quantify the nanoparticles distributed in each layer, the epithelium and submucosa were separated using a combination of ethylenediaminetetraacetic acid (EDTA) and trypsin (2.5 g porcine trypsin and 0.2 g EDTA in 500 mL Hank's balanced salt solution, (Sigma)) with agitation (Vortex-Genie 2, Scientific Industries, Inc.). While trypsin solution is able to enzymatically remove the epithelial layer, EDTA chelates divalent cations, such as Ca^{+2} and Mg^{+2}, that are necessary for cell attachment to the submucosal layer [35]. Agitation provides a physical force that assists in cell lysis and removal of the remaining cells [35].

Aliquots (2mL) of trypsin-EDTA were added to 15 mL polypropylene tubes (Sarstedt, Inc.) containing the tissue explants removed from the diffusion cells, and the samples were incubated on a vortex shaker for 3 hours at room temperature [27]. The tissue explants were removed and the surface was scraped using rubber policeman to complete removal of the epithelial layer. The scraped layer was added to the dispersion while the submucosal tissue was transferred to another empty 15mL polypropylene tube. Cellosolve® acetate was added to both tubes (epithelial dispersion and submucosal tissue) and the samples were incubated for 48 hours in the dark at 37ºC before the fluorescence intensity was obtained from the solvent phase.

Transport Studies Using Pharmacologic Inhibitors

Inhibitor-Mediated Transport Studies

Three pharmacological inhibitors, chlorpromazine, CPZ, (10µg/mL, Sigma) [36], amiloride (260µg/mL, TOCRIS) [23] and m-βCD (5mg/mL, Acros Organic) [36], were used to inhibit nanoparticle uptake in the transport studies [Figure 2.1]. Tissue explants were treated in a similar manner as with the nanoparticle transport studies. Briefly, the explants were equilibrated at 37ºC for one hour with buffer solutions containing one of the three inhibitors in both donor and the receiver chambers. Following the equilibration period, the donor chamber was emptied and replaced with 1ml of 0.1% w/v nanosphere suspension also containing the inhibitor, and the receiver chamber was replaced with 1ml fresh KRB containing the same inhibitor. The transport studies were conducted for 30 or 60 minutes, after which the tissue explants were removed and treated similarly to the untreated transport studies [27].

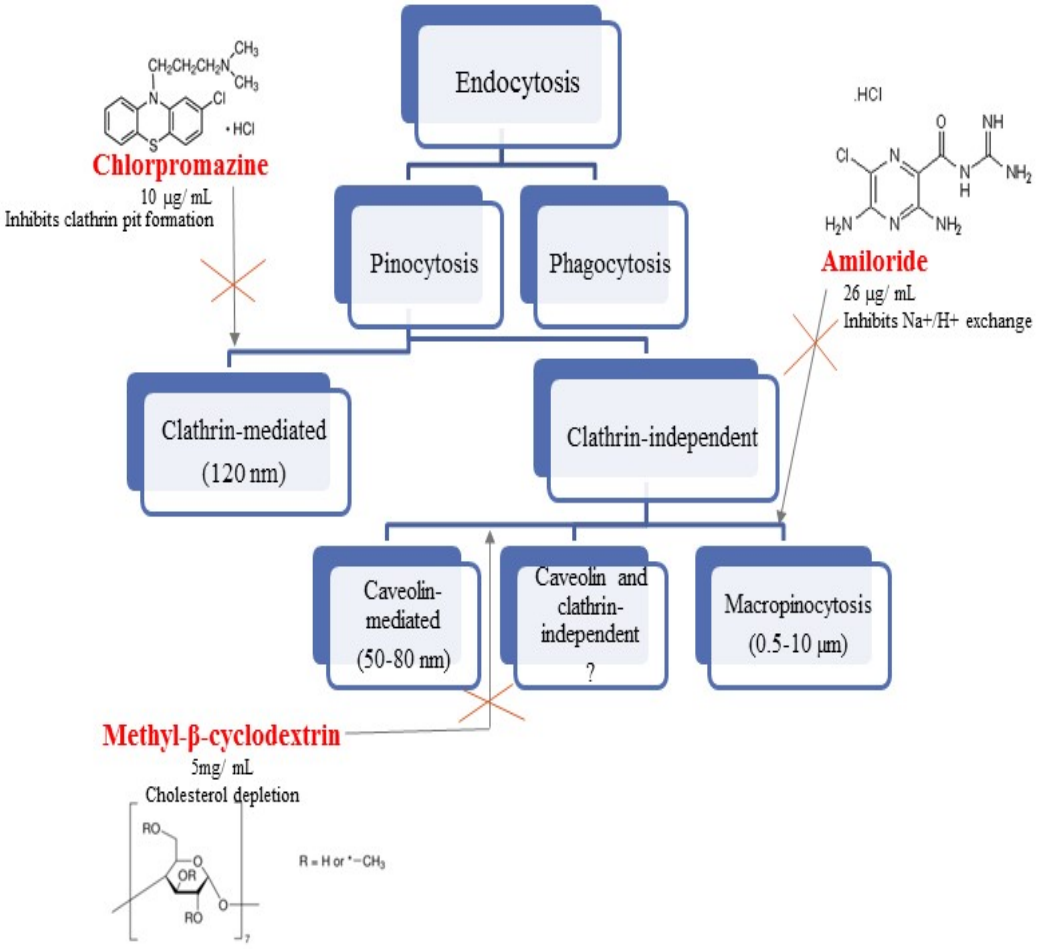

Figure 2.1. Diagram showing the effect of pharmacological inhibitors on endocytic pathways.

Quantification of FluoSpheres® YG Particles

A SpectraMax M5 Multi-Mode spectrofluorimeter was used to measure the fluorescence intensity of the samples. The concentration of the particles was calculated indirectly by measuring the fluorescence intensity of fluorescein, the dye that is loaded within the particles, after dissolving the particles. Particles were dissolved by using Cellosolve® acetate and the dye was released immediately into the medium once the dissolution process started. A period of 48 hours was allowed for complete dissolution and release. The samples were centrifuged for 5min at 5000 xg, and the fluorescence intensity of the dye was measured in the Cellosolve® acetate phase by the spectrofluorimeter [27]. The manufacturer's recommendation for the excitation and emission wavelengths is 505/515 nm. However, for quantitative measurements, the optimum combination of wavelengths that reduce the interference from the overlapping absorption and emission spectra was selected to be 500/560 nm for the excitation and emission spectra, respectively. The emission and excitation spectra are shown in Appendix B [Figures B.3 and B.4].

Each sample was placed in 3mL Cellosolve® acetate and incubated for a period of 48 hours to ensure complete extraction of the dye from the nanoparticles [30]. To determine the concentration of the nanoparticles in the tissue, the fluorescence intensity of the released dye in the Cellosolve® acetate phase was measured and the concentration was indirectly calculated based on a previously established correlation between dye fluorescence intensity and particle concentration [Figure 3.1]. The total mass of the nanoparticles was calculated by multiplying the estimated particle concentration by the volume of the solvent (3mL) that was used for extraction [27]. Finally, the calculated total mass was divided by the mass of the exposed tissue to normalize the uptake with respect to different tissue samples.

Data Analysis

The results from experimental (inhibition) groups were analyzed and compared to the untreated groups (no inhibitor) using a one-tailed, independent-samples Student's t-test. However, the two-tailed, independent samples Student's t-test was used to compare between olfactory and respiratory tissue uptake. The significance level was selected to be $p < 0.05$ for both tests. All the results are displayed as mean $\pm$ standard deviation where n=3 replicates.

CHAPTER III

RESULTS AND DISCUSSION

Particle Size and Zeta Potential Analysis of CM-PNPs

The results of our studies show that the mean diameter of the commercially obtained nanoparticles ranged between 56 nm in Nanopure water to 51 nm in KRB. Zeta potential measurements indicate that the particles are negatively charged in both Nanopure water and KRB. The zeta potential was found to be -47.9 mV in Nanopure water and -20.9 mV in KRB. This lower value in KRB is attributed to the shielding effects of the buffer ions in the suspension. These highly negative values of the zeta potential provide a benefit to keeping the particles dispersed in the medium by increasing the repulsive forces between similar charged surfaces. Table 3.1 displays the results of the particle size and zeta potential measurements in each medium. The particle size distribution results are shown in Appendix B [Figures B.1 and B.2].

Samples		Particle size (nm)	Zeta Potential (mV)
FluoSphere® YG (0.002% W/V, with distilled water)	n=1	57.2	-55.8
	n=1	55	-47.9
FluoSphere® YG (0.002% W/V, with KRB)	n=1	47.4	-35.3
	n=1	55.2	-27.3
FluoSphere® YG (0.002% W/V, with KRB and CPZ)	n=1	54.7	-25.5
	n=1	54.2	-29
FluoSphere® YG (0.002% W/V, with KRB and amiloride)	n=1	88.2	-25.9
	n=1	89.8	-27.1
FluoSphere® YG (0.002% W/V, with KRB and m-βCD)	n=1	53.1	-27.2
	n=1	53	-27.9

Table 3.1. Particle size and surface charge determination for 40 nm CM-PNP in two media. Particle size and zeta potential determined using a Malvern Zetasizer.

Quantitative Calculation of Nanoparticle Uptake from Fluorescence Measurements

A linear correlation between the dye fluorescence intensity and the nanoparticle concentration was established [Figure 3.1]. After removal of the epithelial cell layer using trypsin-EDTA and further extraction of the dye from the epithelial cells and the submucosal tissues, the concentration of the particles was calculated in both the epithelial and submucosal regions of the nasal mucosa by measuring the fluorescence intensity of the dye that was released from the nanoparticles into the Cellosolve® acetate phase. The total mass of the nanoparticles was determined by multiplying the nanoparticle concentration by the solvent volume (3 mL) that was used for extraction. Finally, the total mass of nanoparticles was normalized by the total mass of the tissue region exposed to the nanoparticles. The fluorescence readings and mass calculations are shown in Appendix C. The tissue content of the nanoparticles was determined for full-thickness tissue, the epithelial cells, and the submucosal tissues of the nasal olfactory and respiratory regions both in the presence and absence of pharmacologic inhibitors.

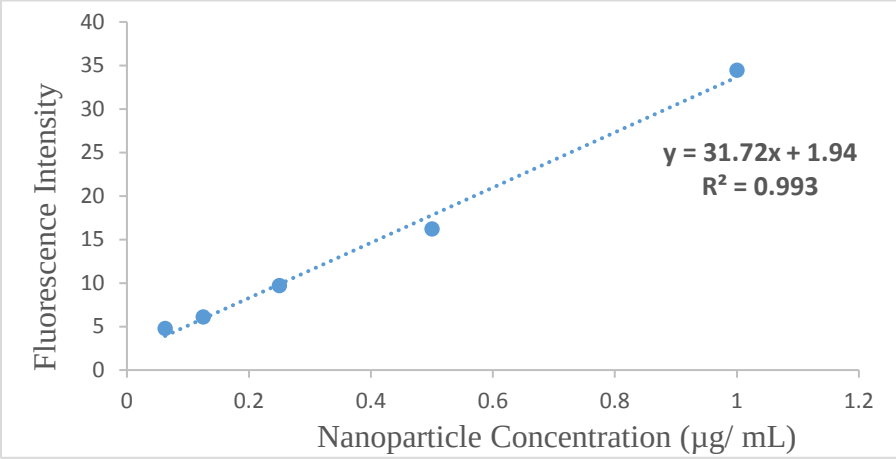

Figure 3.1. Relationship between the fluorescence intensity of the fluorescent dye extracted with Cellosolve® acetate and the 40 nm CM-PSNP w/v concentration. The fluorescence intensity was measured using excitation/emission wavelengths of 500/ 560 nm.

Comparison of the Nanoparticle Content in Isolated Full-thickness Tissues in the Presence and Absence of Endocytic Inhibitors

Assessment of the Uptake of 40 nm Particles by Clathrin-mediated Endocytosis

Chlorpromazine, (CPZ, 10µg/mL), a clathrin-mediated endocytosis inhibitor, was incorporated in the transport medium to examine the effect of clathrin-mediated endocytosis on the uptake of the nanoparticles. In full-thickness olfactory tissues, the uptake of the particles was not significantly reduced in the CPZ-treated group compared to the untreated tissues at the 30 min experimental time [Figure 3.2]. However, continuing the experiment for 60 min showed that the tissue uptake was significantly reduced in the CPZ treated group compared to the untreated tissues [Figure 3.3]. These results show that clathrin-mediated endocytosis results in a time-dependent reduction in the uptake of the nanoparticles by the olfactory tissues.

In the full-thickness respiratory tissues, the uptake of the nanoparticles was found to be significantly lower in the CPZ treated group compared to the untreated group after both 30 and 60 min experimental periods [Figures 3.4 and 3.5]. These results indicate that clathrin-mediated endocytosis has a major contribution to particle uptake in the full-thickness respiratory tissues. These results are in agreement the reported observations of Rejman and Hoekstra who previously reported inhibition of clathrin-mediated endocytosis (via potassium depletion or chlorpromazine) in B16 cells, a melatonin-producing murine skin epithelial cell line, results in lower uptake of 50 nm polystyrene nanoparticles by the cells [37]. Furthermore, these results are also consistent with the report by Lai and Hanes who demonstrated that the internalization of 40 nm CM-PSNPs into human cervical epithelial carcinoma (HeLa) cells via clathrin-coated pits can be inhibited when the cells were treated with chlorpromazine [38].

Assessment of the Uptake of 40 nm Particles by Macropinocytosis

Amiloride (260µg/mL), a macropinocytosis inhibitor, was incorporated in the transport study media to examine the effect of macropinocytosis on the uptake of the polystyrene nanoparticles. In full-thickness olfactory tissues, the uptake of the particles was not significantly lower in the amiloride-treated group compared to the untreated group after a 30 min incubation [Figure 3.2]. However, the uptake was significantly lower after 60 min [Figure 3.3]. These results indicate that at longer time periods (60 min), a significant effect of macropinocytosis on the translocation of the 40 nm nanoparticles through the olfactory tissues occurs.

In full-thickness respiratory tissues, the nanoparticle uptake was significantly lower in the amiloride-treated group as compared to the untreated group after both the 30 and 60 min incubation periods [Figures 3.4 and 3.5]. These results suggest that macropinocytosis in the respiratory tissues plays an important role in the uptake of the nanoparticles. Our observations are in agreement with other studies which have showed that the internalization of 40 nm CM-PSNPs into Hela cells is inhibited in the presence of cytochalasin A (a phagocytosis/macropinocytosis inhibitor) [39].

Assessment of the Uptake of 40 nm Particles by Caveolae-Mediated Endocytosis

M-βCD (5mg/mL), a caveolae-mediated endocytosis inhibitor, was incorporated in the transport studies to examine the effect of caveolae-mediated endocytosis on the uptake of 40 nm particles. In full-thickness olfactory tissues, the uptake of the particles was significantly lower in the m-βCD treated group as compared to the untreated group at both the 30 min and 60 min time periods [Figures 3.2 and 3.3]. These results suggest that caveolae-mediated endocytosis is significantly involved in the uptake process of the nanoparticles in the nasal olfactory tissues.

In full-thickness respiratory tissues, 40 nm particles uptake was not significantly lower in the m-βCD treated group after 30 min [Figure 3.4]. These results are similar to those of Lai and Hanes who reported that the uptake of 40 nm CM-PSNPs by Hela cells was not reduced when the cells were treated with either of the caveolae-mediated inhibitors, genistein or filipin [38]. In our study, however; the uptake was significantly lower than the untreated group after 60 min [Figure 3.5]. These results indicate that the caveolae-mediated pathway may play a limited role in the uptake of the nanoparticles by the nasal respiratory tissues.

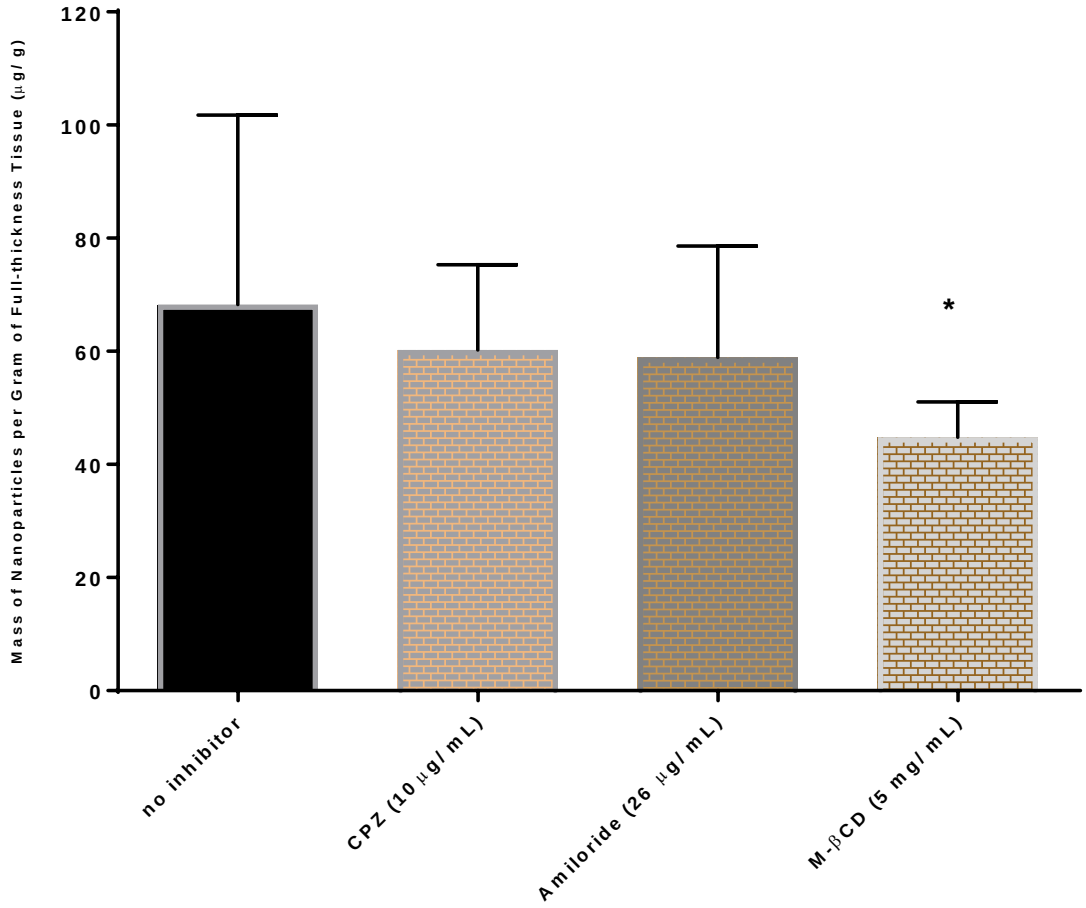

Figure 3.2. Effects of inhibitors of endocytosis on the uptake of 40 nm CM-PNPs in full-thickness olfactory mucosal tissues after a 30 min incubation. Results are shown as the mean ± SD, n=3. Each endocytic inhibitor was compared independently to the untreated (no inhibitor) tissues using the one-tailed, independent samples Student's t-test. (*) denotes significant statistical difference, $p < 0.05$.

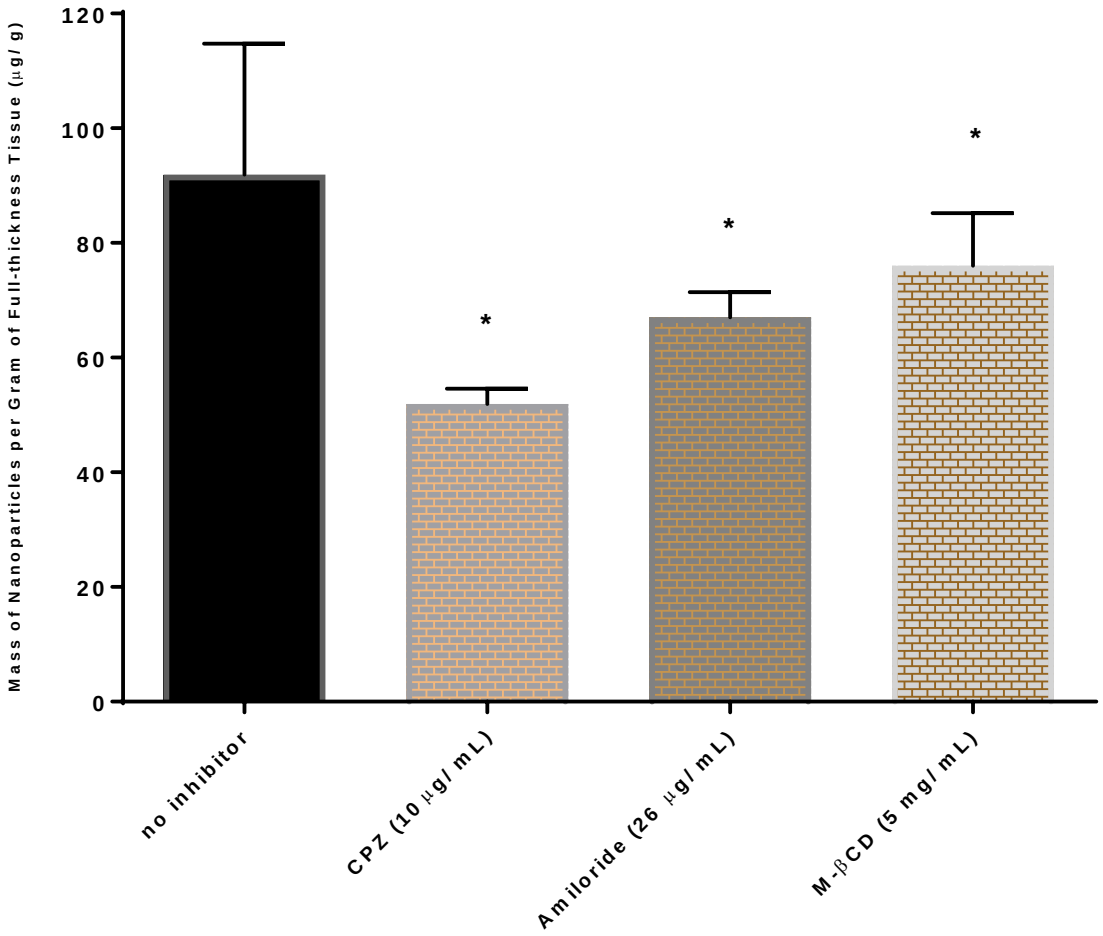

Figure 3.3. Effects of inhibitors of endocytosis on the uptake of 40 nm CM-PNPs in full-thickness olfactory mucosal tissues after a 60 min incubation. Results are shown as the mean ± SD, n=3. Each endocytic inhibitor was compared independently to the untreated (no inhibitor) tissues using the one-tailed, independent samples Student's t-test. (*) denotes significant statistical difference, $p < 0.05$.

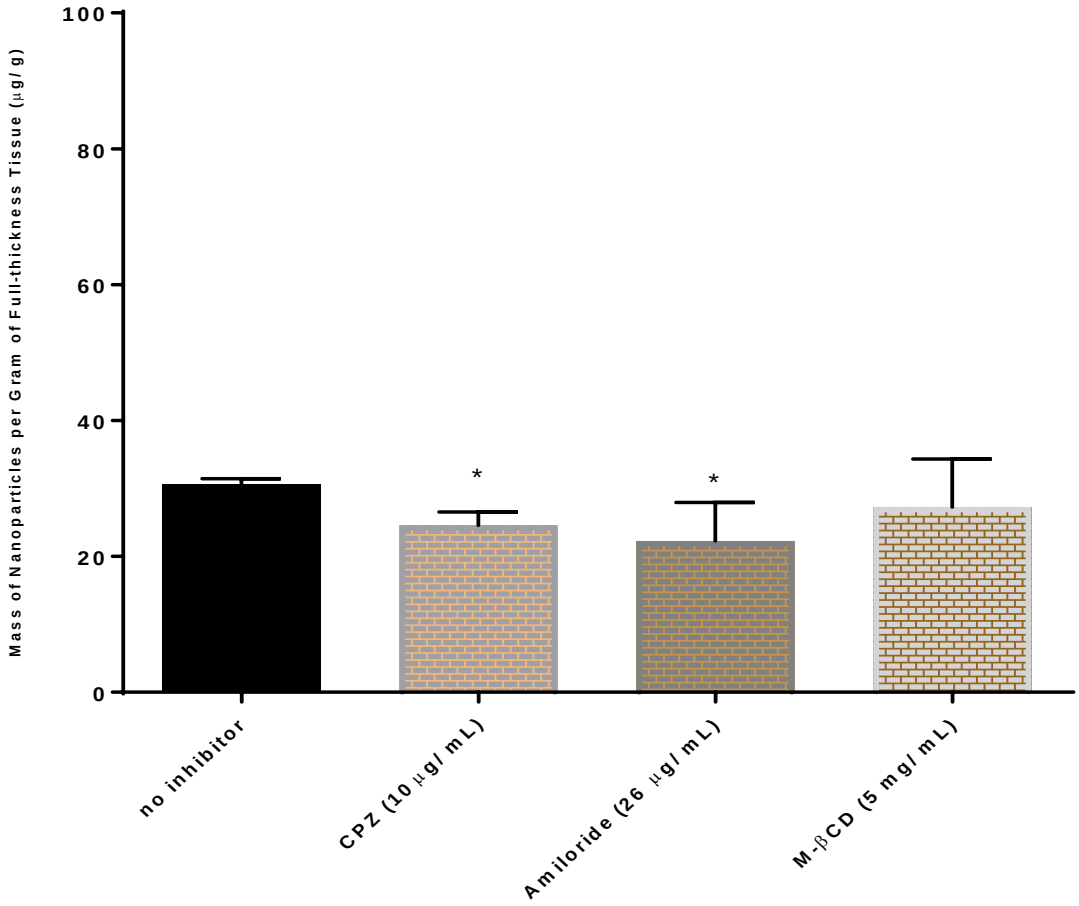

Figure 3.4. Effects of inhibitors of endocytosis on the uptake of 40 nm CM-PNPs in full-thickness respiratory mucosal tissues after a 30 min incubation. Results are shown as the mean ± SD, n=3. Each endocytic inhibitor was compared independently to the untreated (no inhibitor) tissues using the one-tailed, independent samples Student's t-test. (*) denotes significant statistical difference, $p < 0.05$.

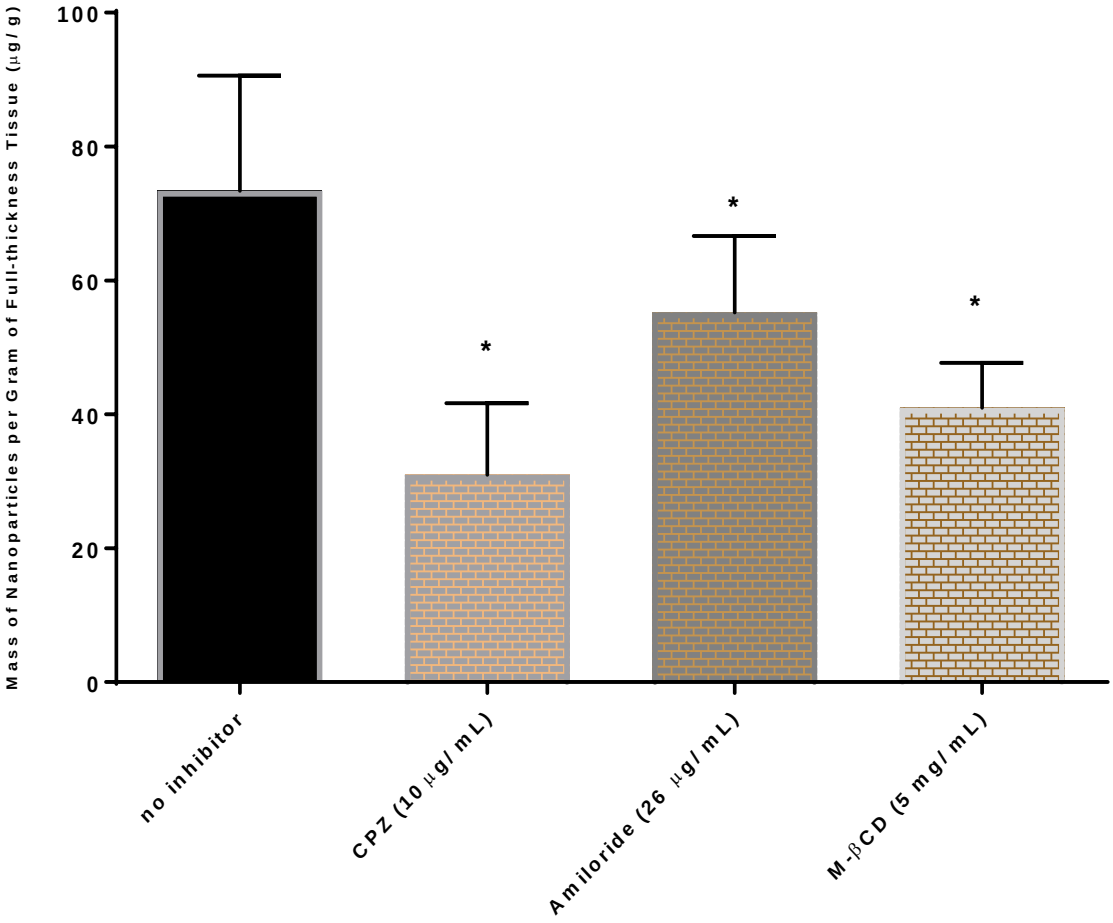

Figure 3.5. Effects of inhibitors of endocytosis on the uptake of 40 nm CM-PNPs in full-thickness respiratory mucosal tissues after a 60 min incubation. Results are shown as the mean ± SD, n=3. Each endocytic inhibitor was compared independently to the untreated (no inhibitor) tissues using the one-tailed, independent samples Student's t-test. (*) denotes significant statistical difference, $p < 0.05$.

Comparison of 40 nm Nanoparticle Uptake in Isolated Epithelial Layers

The nasal mucosal tissues were de-epithelized using trypsin-EDTA with agitation to quantify the amount of nanoparticles in the epithelial cells. The dissociated epithelial cells were collected in a 15 mL polypropylene tube and the remaining submucosal tissue was transferred into another tube for further treatment. The nanoparticle exposure experiments were carried out for 30 and 60 minutes.

At all times and under all conditions of the nasal olfactory and respiratory tissues, In the nasal olfactory and respiratory tissues, the mass of the nanoparticles in the epithelial layer after both 30 and 60 min experimental periods was found to be higher compared to the submucosal tissues [Figures 3.6-3.9].

Assessment of the Uptake of 40 nm Particles by Clathrin-mediated Endocytosis

As with the full-thickness nasal olfactory tissues, the uptake of the nanoparticles by the nasal olfactory epithelium was not significantly lower in the presence of CPZ than the untreated group at the 30 min incubation [Figure 3.6]. Yet, for the longer incubation period of 60 min, the uptake was significantly lower in both the full-thickness tissues and the epithelial cells of the nasal olfactory tissues [Figure 3.7].

The uptake of the nanoparticles by the epithelial cells of the nasal respiratory tissues was significantly lower following CPZ treatment at both the 30 min and the 60 min experimental periods compared to the untreated tissues [Figures 3.8 and 3.9]. These results are also similar to those observed in the full-thickness nasal respiratory tissues suggesting that this route is a major endocytic pathway for the uptake of the nanoparticles.

Assessment of the Uptake of 40 nm Particles by Macropinocytosis

In nasal olfactory tissues, the uptake of the nanoparticles by the epithelial cells after 30 min was not significantly lower in the amiloride treated group as compared to the untreated group [Figure 3.7]. On the other hand, the uptake of the nanoparticles was significantly lower after the 60 min incubation time [Figure 4.8]. These results were similar to the results observed in full-thickness nasal olfactory tissues.

When the respiratory epithelium was treated with amiloride for both 30 and 60 min, the uptake was significantly lower than the untreated groups at both times [Figures 3.8 and 3.9]. Similar observations were noticed in the full-thickness nasal respiratory tissues.

Assessment of the Uptake of 40 nm Particles by Caveolae-Mediated Endocytosis

As observed with the uptake by the full-thickness nasal olfactory tissues, the uptake of the 40 nm nanoparticles after both 30 and 60 min was significantly lower in the m-βCD treated group compared to the untreated group [Figures 4.6 and 3.7].

The uptake of the nanoparticles by the epithelial cells was significantly lower after 30 min incubation than in untreated tissues [Figure 3.8]. After a 60 min incubation, similar to the full-thickness m-βCD treated nasal respiratory tissues, the uptake was significantly lower in the epithelial cells [Figure 3.9]. These results suggest that caveolae-mediated endocytosis plays a time-dependent role in 40 nm nanoparticle uptake by the nasal respiratory epithelial cells.

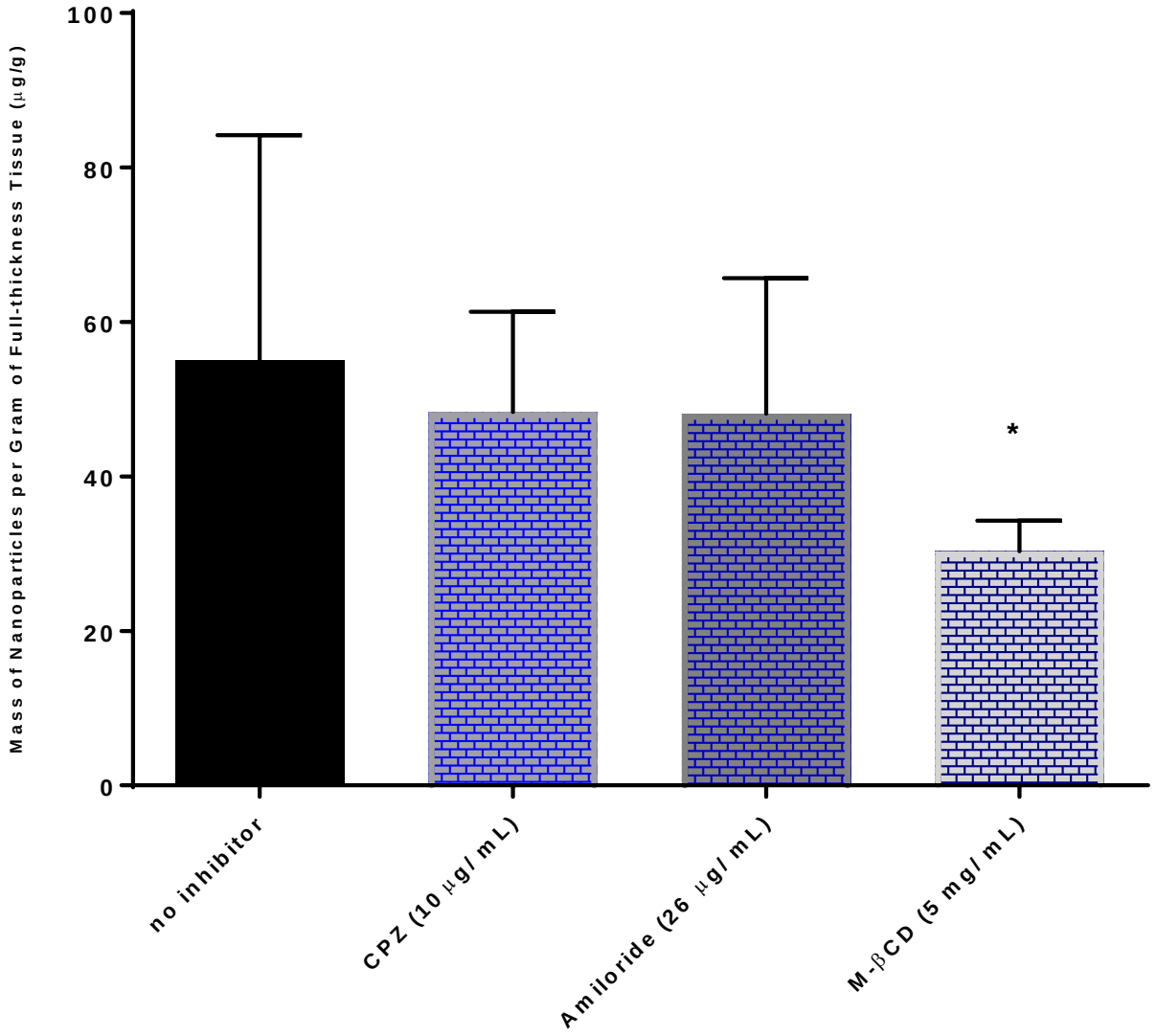

Figure 3.6. Effects of inhibitors of endocytosis on the 30 min uptake of 40 nm CM-PNPs by the epithelial cells of the olfactory mucosa. Results are shown as the mean ± SD, n=3. Each individual group endocytic inhibitor was statistically compared to the no inhibitor group using the one-tailed, independent samples Student's t-test. (*) denotes significant statistical difference, $p < 0.05$.

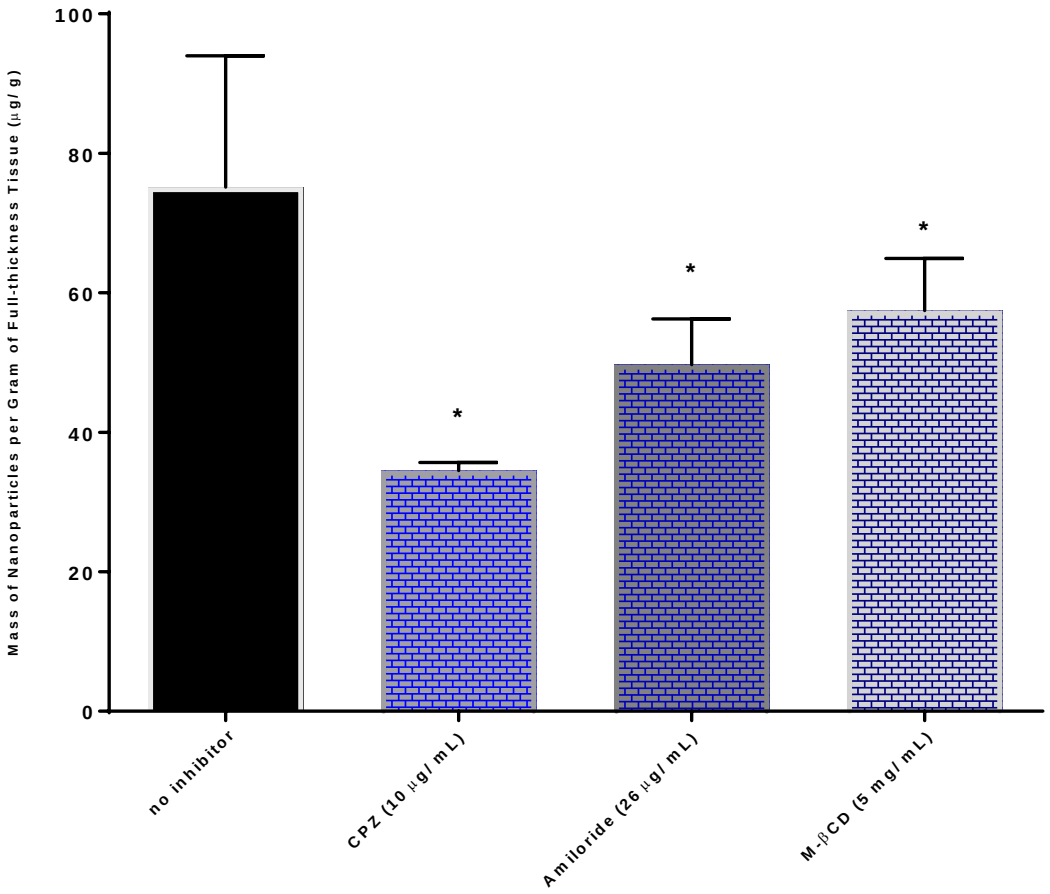

Figure 3.7. Effects of inhibitors of endocytosis on the 60 min uptake of 40 nm CM-PNPs by the epithelial cells of the olfactory mucosa. Results are shown as the mean ± SD, n=3. Each individual group endocytic inhibitor was statistically compared to the no inhibitor group using the one-tailed, independent samples Student's t-test. (*) denotes significant statistical difference, $p < 0.05$.

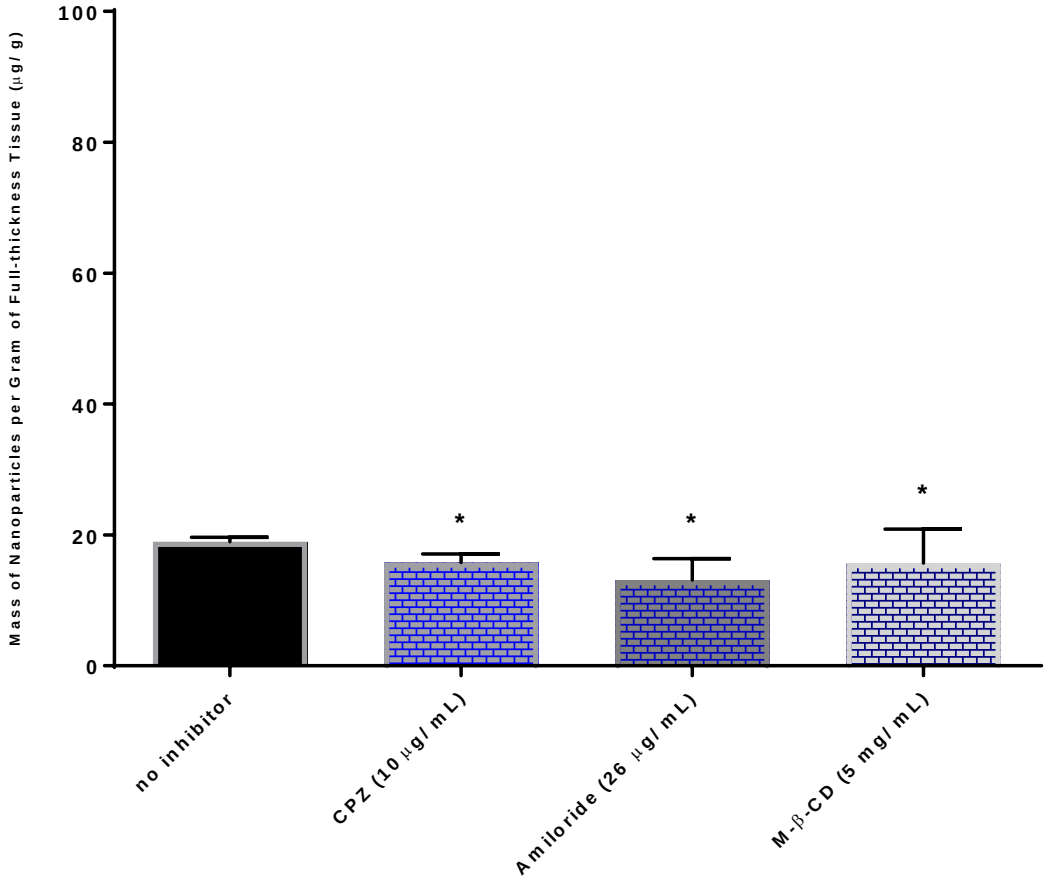

Figure 3.8. Effects of inhibitors of endocytosis on the 30 min uptake of 40 nm CM-PNPs by the epithelial cells of the respiratory mucosa. Results are shown as the mean ± SD, n=3. Each individual group endocytic inhibitor was statistically compared to the no inhibitor group using the one-tailed, independent samples Student's t-test. (*) denotes significant statistical difference, $p < 0.05$.

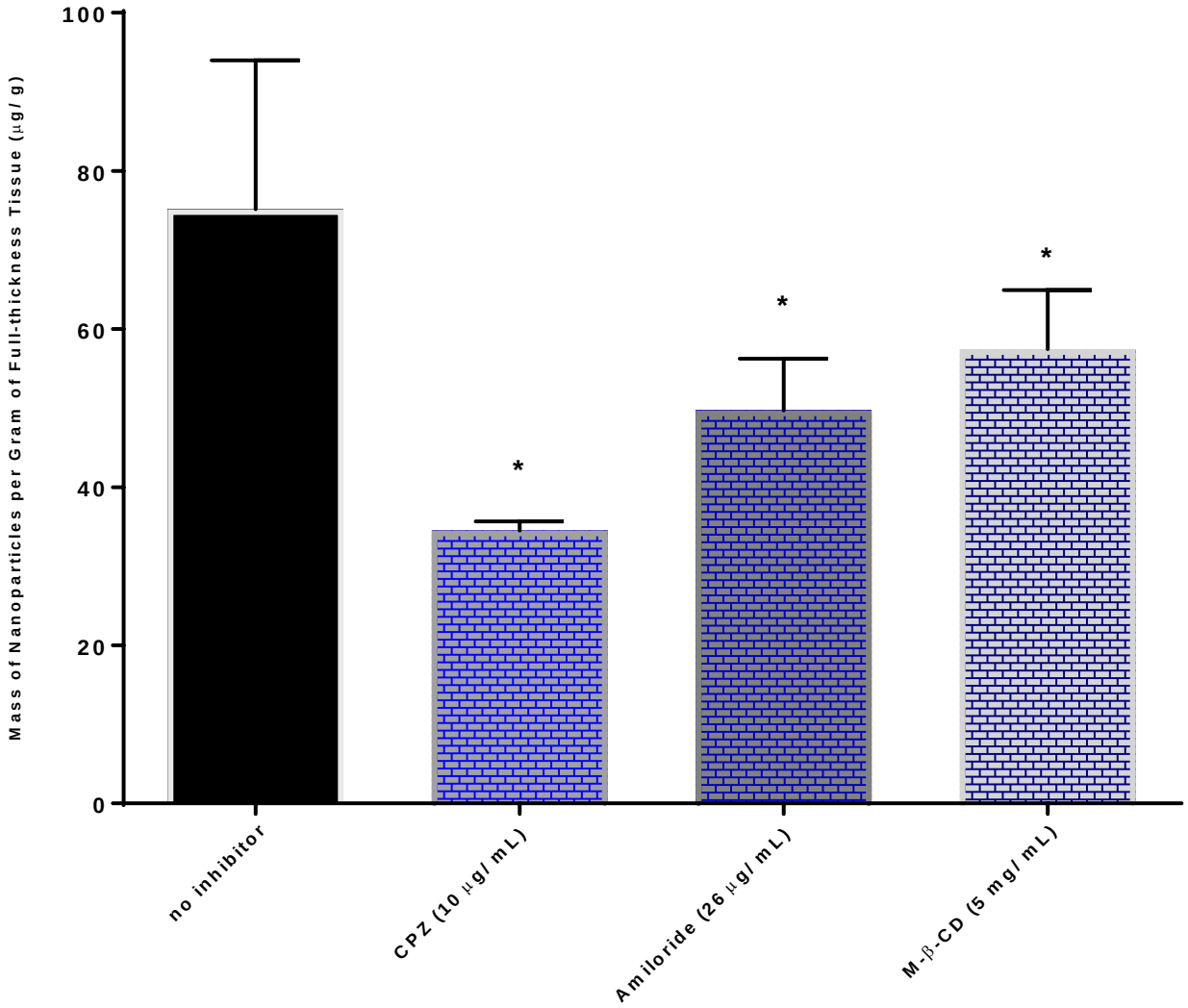

Figure 3.9. Effects of inhibitors of endocytosis on the 60 min uptake of 40 nm CM-PNPs by the epithelial cells of the respiratory mucosa. Results are shown as the mean ± SD, n=3. Each individual group endocytic inhibitor was statistically compared to the no inhibitor group using the one-tailed, independent samples Student's t-test. (*) denotes significant statistical difference, $p < 0.05$.

Comparison of Nanoparticle Content in the Nasal Submucosa

The lamina propria (submucosal region) is highly perfused with blood vessels that can carry absorbed nanoparticles into the blood stream. Thus, it provides a potential delivery pathway to the systemic circulation. We assume that the main pathway by which the nanoparticles can be translocated to the submucosal tissues is via transcytosis across the basal membrane of the epithelial cells following initial endocytosis across the apical membrane. In order to evaluate the role of the endocytic uptake pathways on the distribution of nanoparticles within the submucosal region, the number of the particles in the submucosal region was also determined in the presence and absence of endocytic inhibitors.

Assessment of the Uptake of 40 nm Particles by Clathrin-mediated Endocytosis

In the olfactory tissues, the translocation of the 40 nm particles to the submucosa was not significantly lower in the CPZ treated group as compared to the untreated group after either 30 or 60 min incubation [Figures 3.10 and 3.11]. Although a similar result was obtained for the 30 min transport period in full-thickness tissues, the uptake was significantly lower in the epithelial cells of the CPZ treated group after a 60 min incubation. This observation suggests that an extended time period is required for CPZ to exert its inhibitory effect on the apical surface of the epithelial cells but it has no further effect on the translocation of the particles into the submucosal region.

After treating the nasal respiratory explants with CPZ and incubating for 30 min, the numbers of 40 nm particles in the submucosa was significantly lower than in the untreated tissues [Figure 3.12]. However, unexpectedly, the amount of the particles in the submucosal tissues after 60 min was not significantly lower than in the untreated group [Figure 3.13], but, at the same time, the amount in the epithelial cells was reduced.

Assessment of the Uptake of 40 nm Particles by Macropinocytosis

In the olfactory tissues, the translocation of the particles to the submucosa was not significantly lower in the amiloride treated group compared to the untreated group after both 30 min and 60 min [Figures 3.10 and 3.11]. These results indicate that macropinocytosis does not play a significant role in the translocation of the particles from the epithelial layer to the submucosal region. However, when the respiratory tissues were treated with amiloride, the amounts of nanoparticles in the submucosa was significantly lower than the untreated group after both 30 and 60 min incubation period [Figures 3.12 and 3.13]. It appears the significantly lower nanoparticle content in the submucosa is attributed to the inhibitory effect of amiloride on the epithelial cells where macropinocytosis was shown to result in a significantly lower uptake in the epithelial cells.

Assessment of the Uptake of 40 nm Particles by Caveolae-Mediated Endocytosis

In the submucosal regions of the olfactory and respiratory tissues, the translocation of the nanoparticles to the submucosal region was not significantly lower in the m-βCD treated group compared to the untreated group after both 30 and 60 min incubation [Figures 3.10-3.13]. Insignificant amounts of nanoparticles reached the submucosa utilizing this pathway.

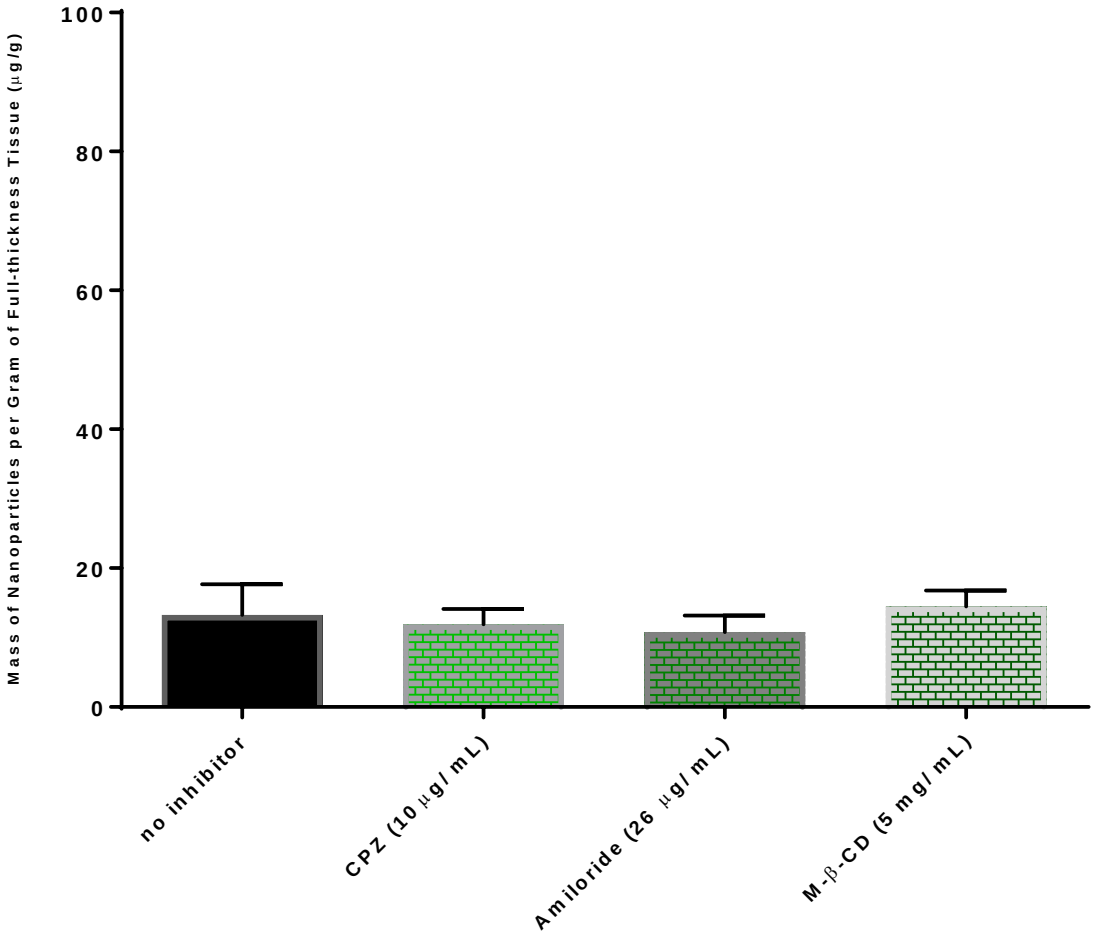

Figure 3.10. Effects of inhibitors of endocytosis on the 30 min uptake of 40 nm CM-PNPs by the submucosal region of the olfactory mucosa. Results are shown as the mean ± SD, n=3. Each specific endocytic inhibitor was statistically compared with the no inhibitor (untreated) group using the one-tailed, independent samples Student's t-test.

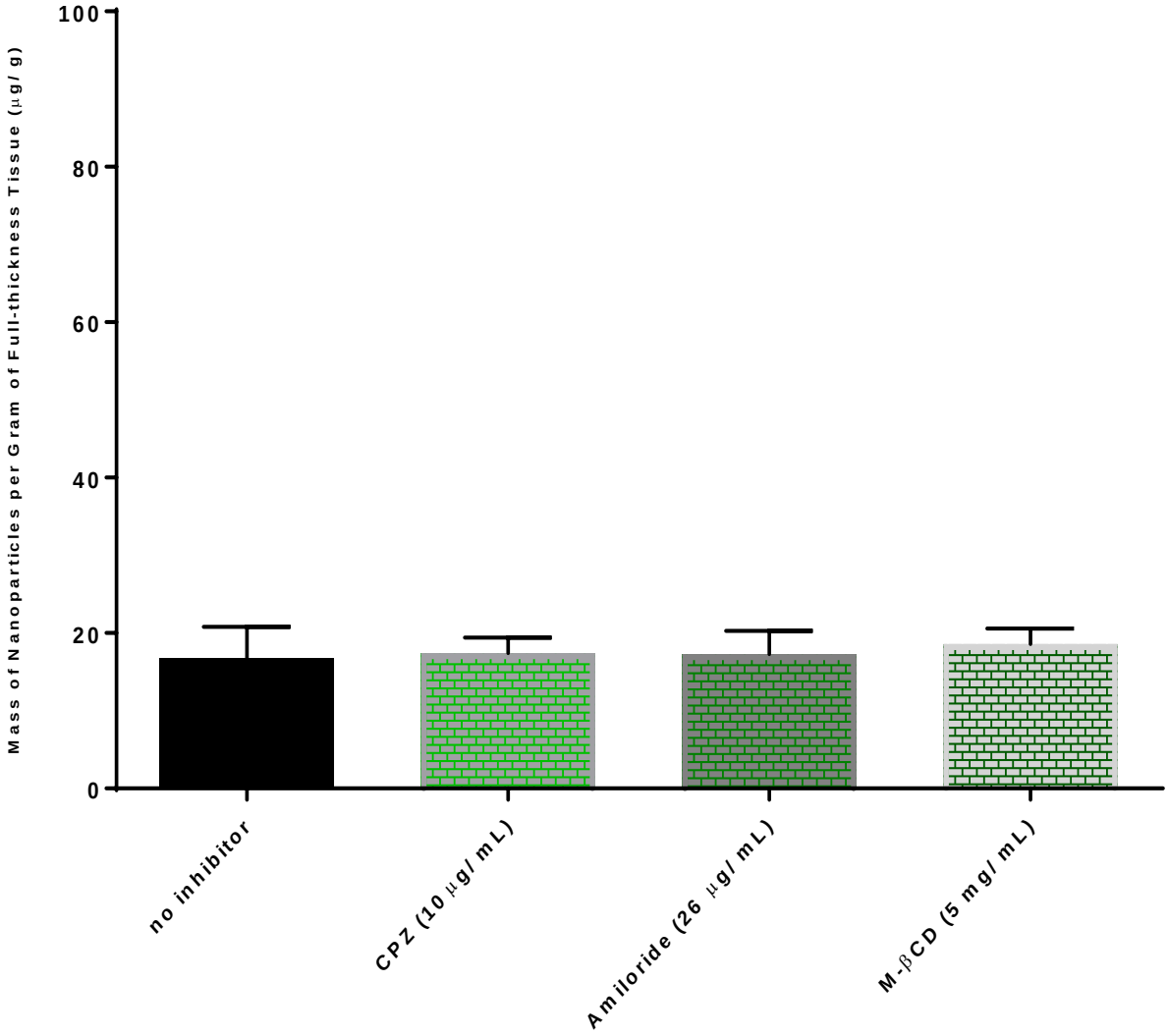

Figure 3.11. Effects of inhibitors of endocytosis on the 60 min uptake of 40 nm CM-PNPs by the submucosal region of the olfactory mucosa. Results are shown as the mean ± SD, n=3. Each specific endocytic inhibitor was statistically compared with the no inhibitor (untreated) group using the one-tailed, independent samples Student's t-test.

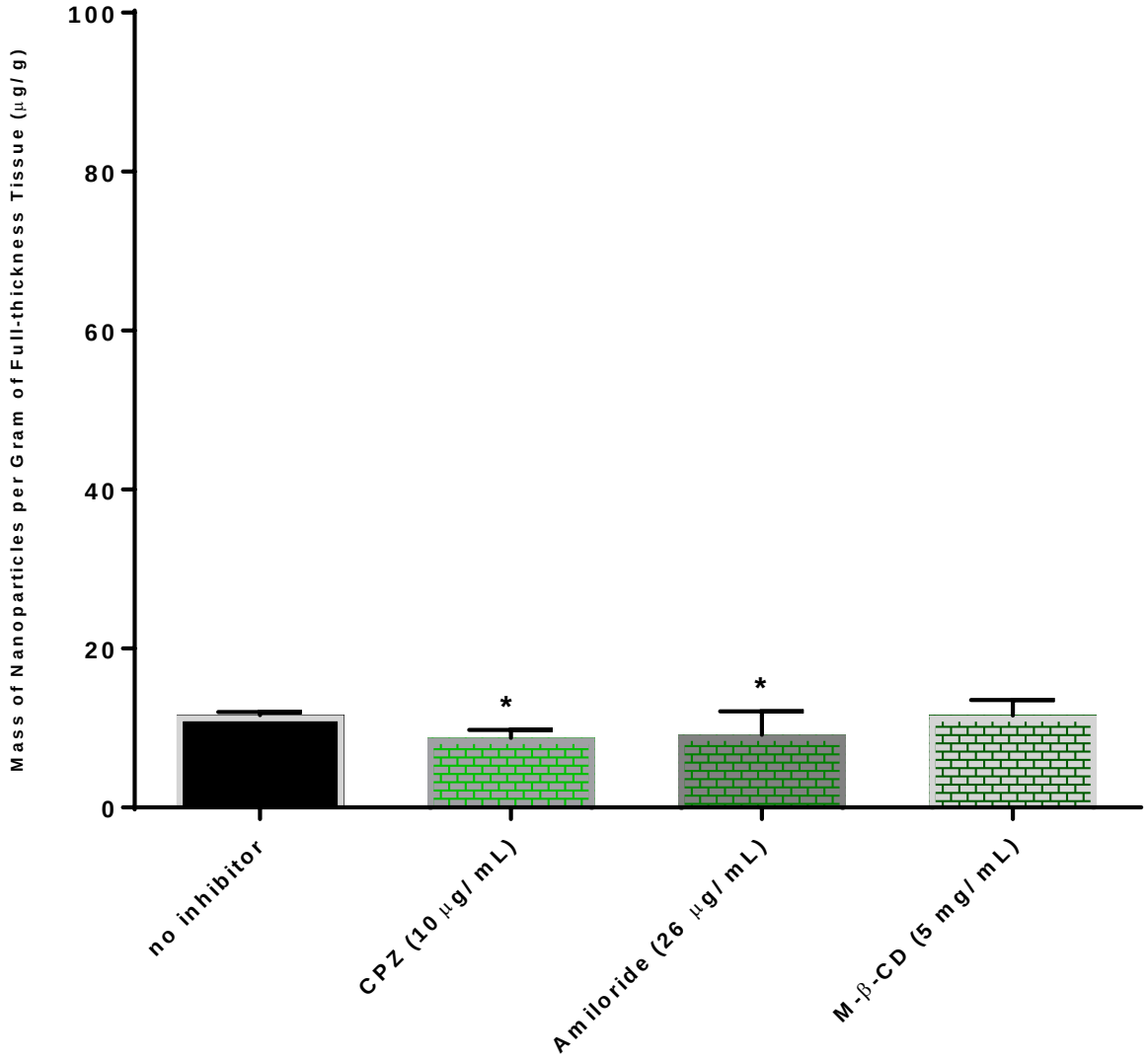

Figure 3.12. Effects of inhibitors of endocytosis on the 30 min uptake of 40 nm CM-PNPs by the submucosal region of the respiratory mucosa. Results are shown as the mean ± SD, n=3. Each specific endocytic inhibitor was statistically compared with the no inhibitor (untreated) group using the one-tailed, independent samples Student's t-test. (*) denotes significant statistical difference, $p < 0.05$.

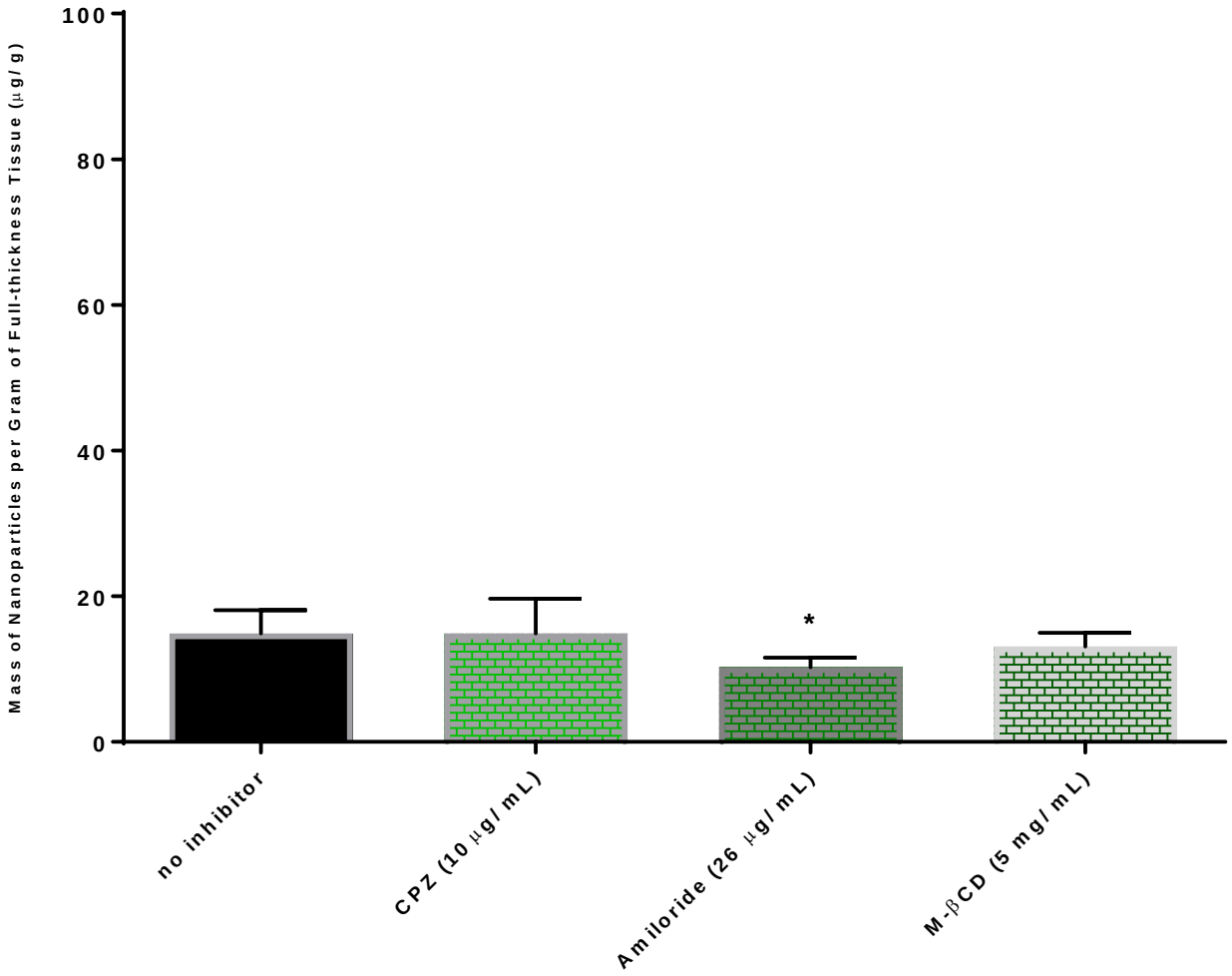

Figure 3.13. Effects of inhibitors of endocytosis on the 60 min uptake of 40 nm CM-PNPs by the submucosal region of the respiratory mucosa. Results are shown as the mean ± SD, n=3. Each specific endocytic inhibitor was statistically compared with the no inhibitor (untreated) group using the one-tailed, independent samples Student's t-test. (*) denotes significant statistical difference, $p < 0.05$.

Comparison of the Nanoparticle Content between Isolated Olfactory and Respiratory Epithelial and Submucosal Layers

Comparisons of the differences between the endocytic activity in the olfactory and respiratory epithelial and submucosal layers were made to evaluate mucosal region-specific particle uptake pathways.

Assessment of the Uptake of the Particles in Untreated and Inhibitory Studies

After both 30 and 60 min incubations, the amounts of nanoparticles in the olfactory epithelial cells, submucosal regions, and full-thickness tissues were found to be higher than those within the comparable regions of the respiratory explants. Also, the uptake of the nanoparticles was always greater in the olfactory explants than in the respiratory explants when endocytic inhibitors were included in the media [Figures 3.14-3.17]. These results indicate that olfactory mucosa has a greater ability to transport the nanoparticles and is less affected by endocytic inhibitors than the respiratory mucosa.

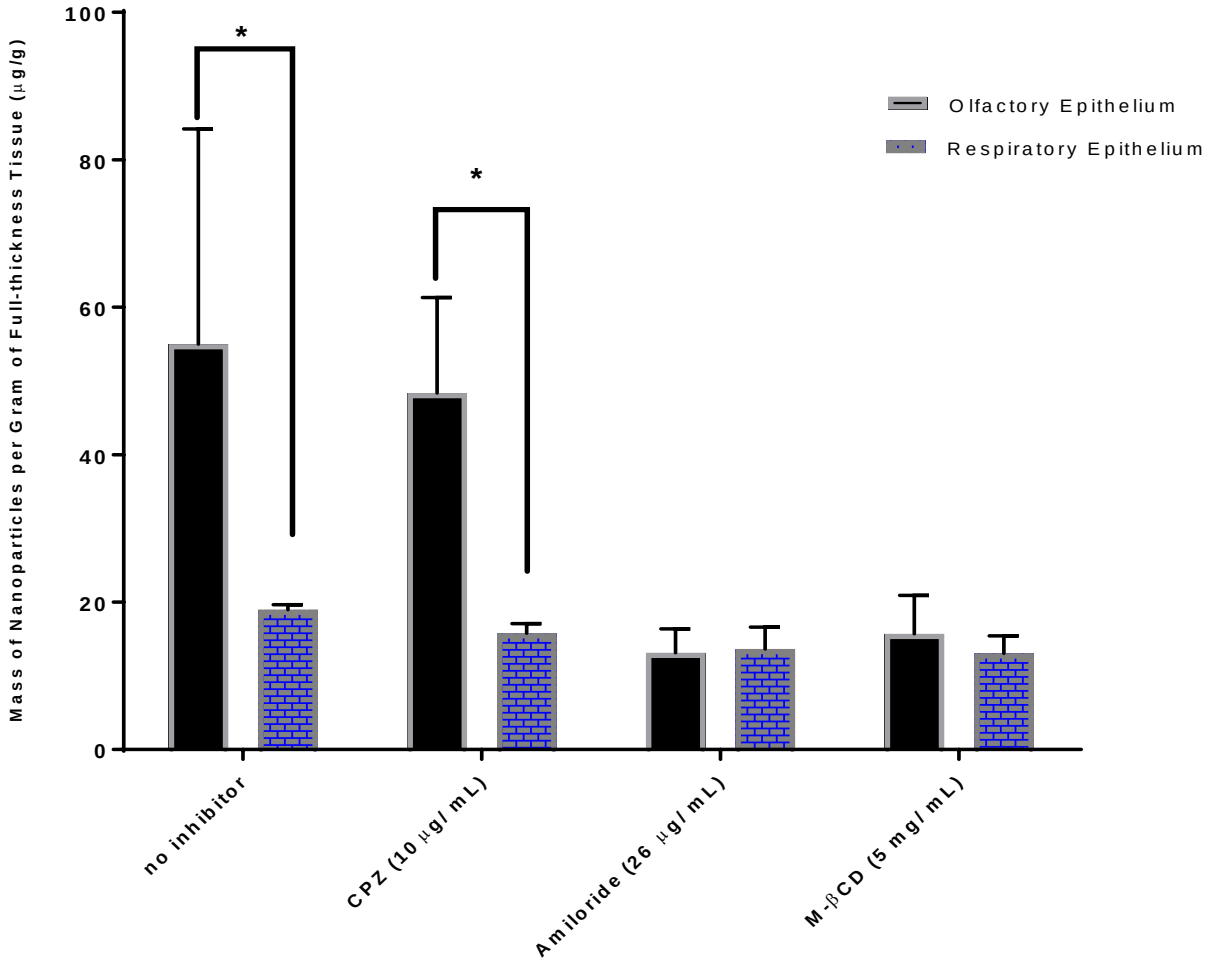

Figure 3.14. Comparison of the 30 min uptake of 40 nm CM-PNPs by the nasal olfactory and respiratory epithelium and the effect of endocytic inhibitors. Results are shown as the mean ± SD, n=3. Each specific olfactory tissue group (with or without inhibitor) was statistically compared with respiratory tissue group of similar treatment using the two-tailed, independent samples Student's t-test. (*) denotes significant statistical difference, $p < 0.05$.

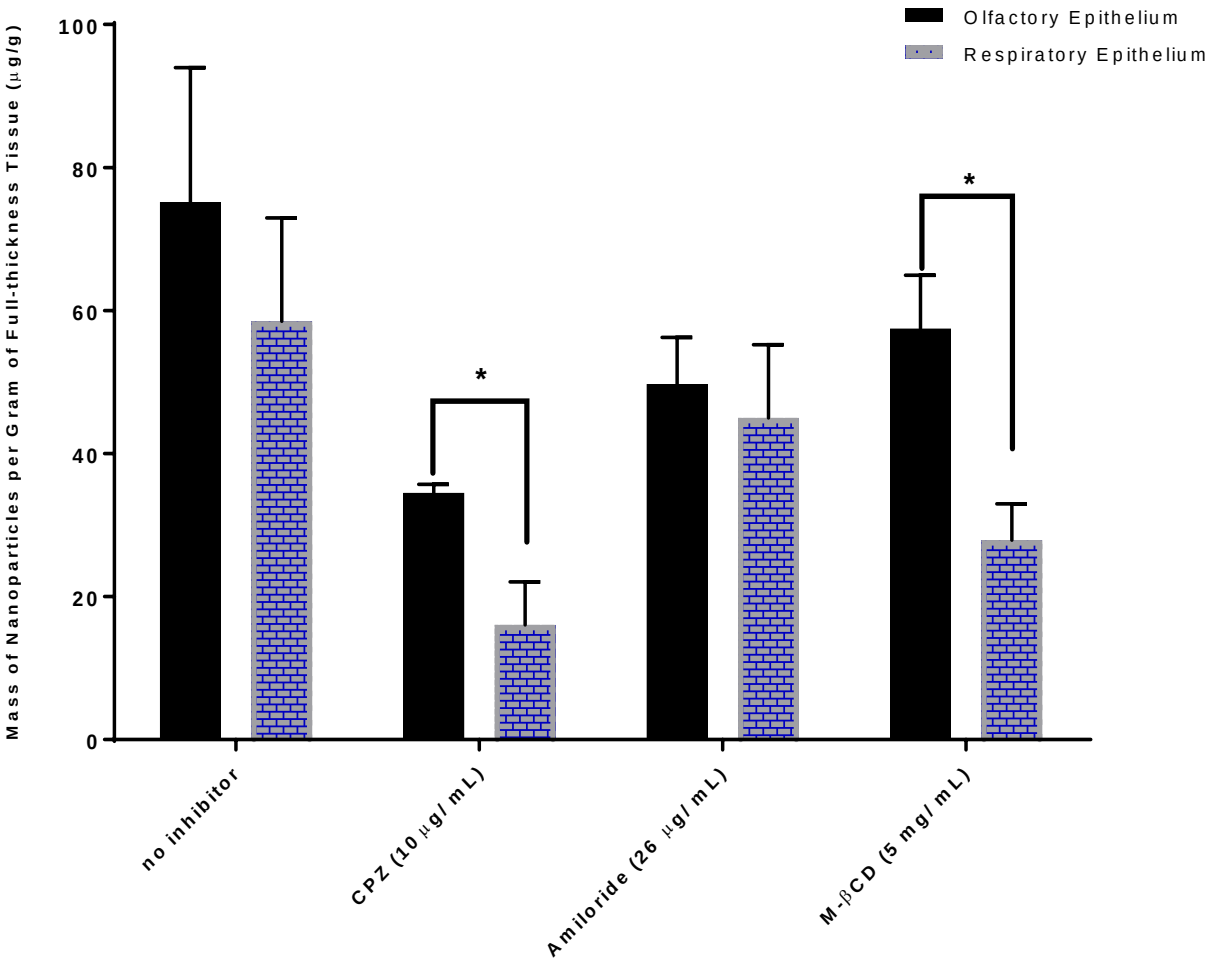

Figure 3.15. Comparison of the 60 min uptake of 40 nm CM-PNPs by the nasal olfactory and respiratory epithelium and the effect of endocytic inhibitors. Results are shown as the mean ± SD, n=3. Each specific olfactory tissue group (with or without inhibitor) was statistically compared with respiratory tissue group of similar treatment using the two-tailed, independent samples Student's t-test. (*) denotes significant statistical difference, $p < 0.05$.

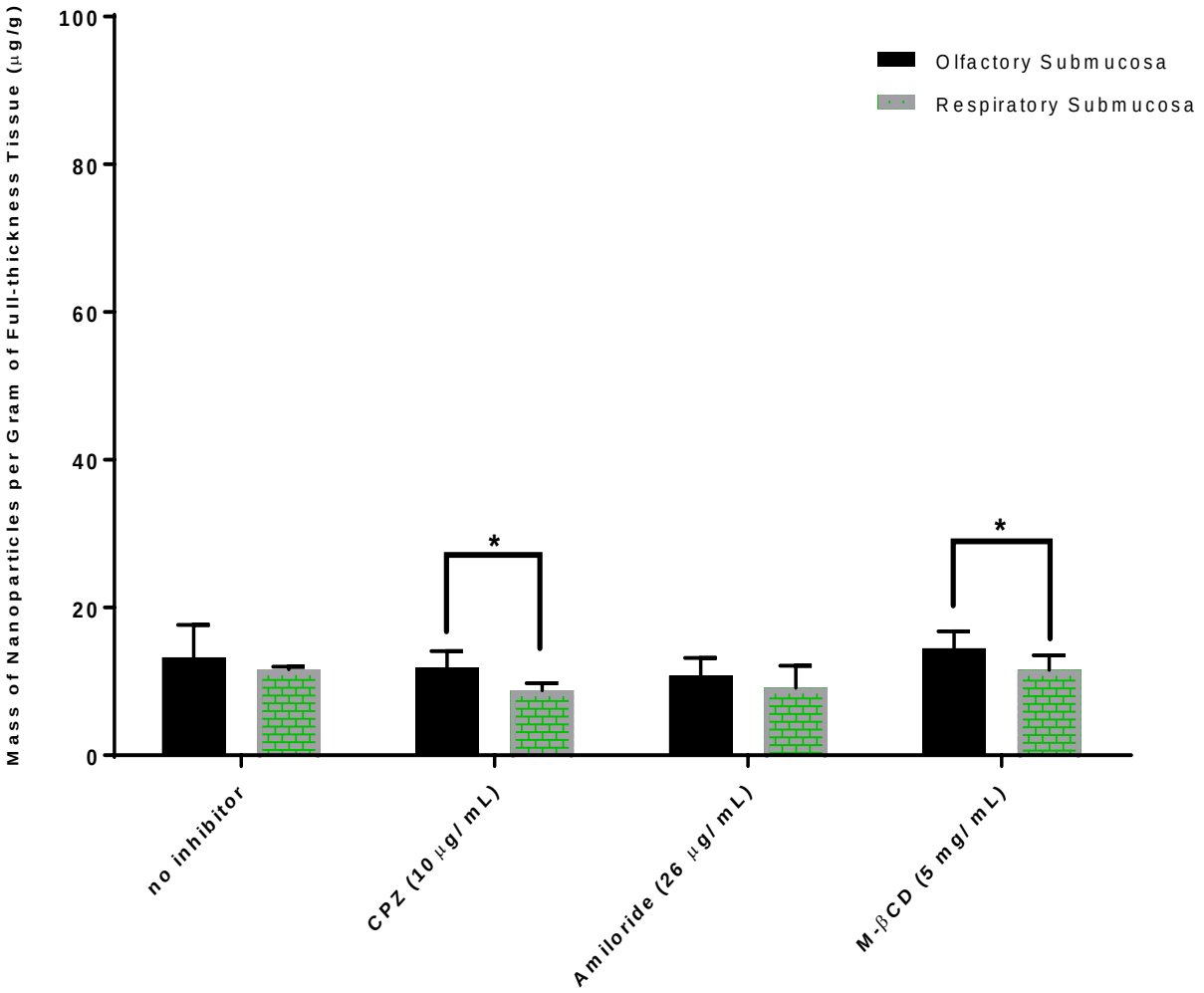

Figure 3.16. Comparison of the 30 min uptake of 40 nm CM-PNPs by the olfactory and respiratory nasal submucosa and the effect of endocytic inhibitors. Results are shown as the mean ± SD, n=3. Each specific olfactory tissue group (with or without inhibitor) was statistically compared with respiratory tissue group of similar treatment using the two-tailed, independent samples Student's t-test. (*) denotes significant statistical difference, $p < 0.05$.

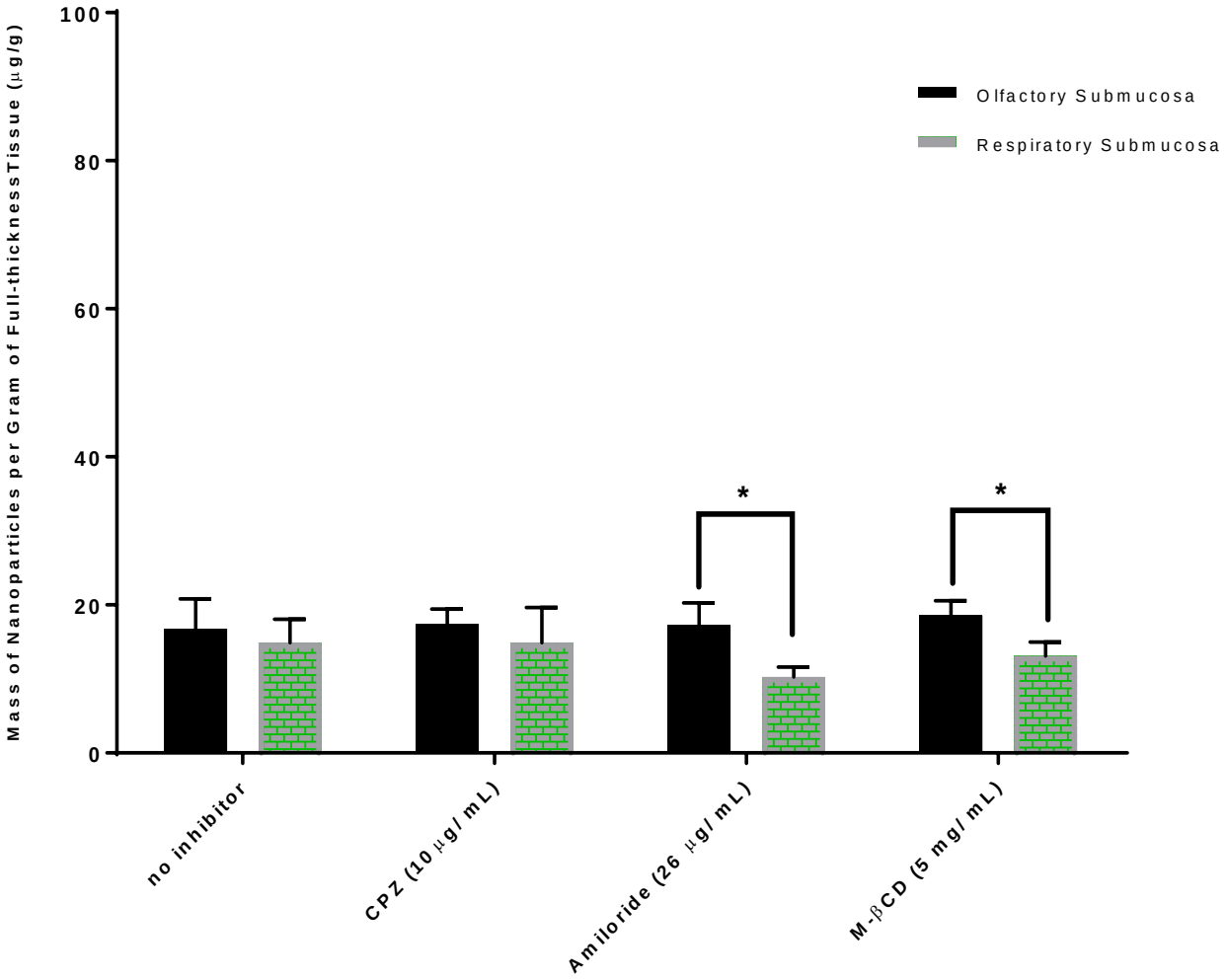

Figure 3.17. Comparison of the 60 min uptake of 40 nm CM-PNPs by the olfactory and respiratory nasal submucosa and the effect of endocytic inhibitors. Results are shown as the mean ± SD, n=3. Each specific olfactory tissue group (with or without inhibitor) was statistically compared with respiratory tissue group of similar treatment using the two-tailed, independent samples Student's t-test. (*) denotes significant statistical difference, $p < 0.05$.

CHAPTER IV

CONCLUSIONS AND FUTURE DIRECTION

Conclusions

Nanoparticle-containing drug delivery systems hold a promising future for improving drug therapy. However, their application in medical therapy requires a further understanding of nanoparticle disposition in biological systems. One of the most important issues in nanoparticle delivery is defining the pathways by which these particles cross cell membranes and distribute within tissues. It is essential to fully understand the mechanisms by which nanoparticles cross cell membranes. Furthermore, it is important to characterize each pathway by which nanoparticles can be translocated through cell and tissues.

These transport studies used different pharmacologic, endocytic inhibitors to show that 40 nm fluorescently-labeled, CM-PNPs were transported by multiple endocytic pathways across the nasal tissues. In the nasal olfactory tissues, the particles were translocated mainly by caveolae-mediated endocytosis. Moreover, this pathway, as well as macropinocytosis and clathrin-mediated endocytosis, were shown to play a significant role in the long-term (60 min) translocation of the particles across the nasal olfactory tissues. In the nasal respiratory tissues, the particles were translocated utilizing all three endocytic pathways over the short and long uptake exposure periods.

In both the olfactory and respiratory nasal mucosa, the submucosal content of the nanoparticles was about one third of the total content of the full-thickness tissues in the presence or absence of inhibitors. Since the submucosal nanoparticle levels were low and nearly constant, we conclude that, and as anticipated, endocytosis has a minimal impact in translocating the 40 nm, CM-PSNPs into the submucosal tissues.

Finally, the nasal olfactory tissues showed nearly a 2-fold higher uptake of nanoparticles than the nasal respiratory tissues. These results indicate that the olfactory cells have a greater ability to transport nanoparticles and this may be of significant value in delivering drugs the central nervous system.

Future Directions

The Nasal Associated Lymphoid Tissue (NALT) is present primarily within the nasal respiratory tissues and is an important component of the nasal immune system that provides local defense to the nasal mucosa. Upon intranasal vaccination, NALT acts as an immune inductive site that plays a major role in antigen recognition and immune activation. However, NALT is not well-characterized and the transport pathways by which nanoparticles transport to this tissue are not well understood.

Our future work will be directed toward characterizing the uptake pathways by which nanoparticles translocate to the NALT to provide an improved understanding of the role of the NALT as a mucosal immune inductive site for vaccination.

APPENDIX A

PRAPARATION OF KREBS RINGER BICARBONATE BUFFER (KRB) [27]

Krebs Ringer Bicarbonate buffer (KRB) used in the diffusion studies includes:

(A) 123.8 mM sodium chloride (Fisher Scientific, Fair Lawn, New Jersey)

(B) 4.56 mM potassium chloride (EM Science, Gibbstown, New Jersey)

(C) 1.67 mM magnesium chloride (Fisher Scientific, Fair Lawn, New Jersey)

(D) 1.5 mM monobasic sodium phosphate (Fisher Scientific, Fair Lawn, New Jersey)

(E) 0.7 mM dibasic sodium phosphate (Spectrum Chemical Corp., Gardena, California)

(F) 10 mM dextrose (EM Science, Gibbstown, New Jersey)

(G) 1.2 mM calcium chloride (Fisher Scientific, Fair Lawn, New Jersey)

(H) 15 mM sodium bicarbonate (EM Science, Gibbstown, New Jersey)

All of the chemicals were dissolved, except for calcium chloride, in 900 mL of Nanopure water. Carbogen (5% carbon dioxide USP with 95% oxygen USP) was bubbled through the solution for 10 min in order to lower the pH slightly, and then calcium chloride was added. Adjustments were made by adding 1N hydrochloric acid or sodium hydroxide to a final value of pH = 7.4. Finally, the volume of the solution was made up to 1000 mL with Nanopure water.

APPENDIX B

Size Distribution Results of 40 nm CM-PSNPs Suspended in Two Different Media

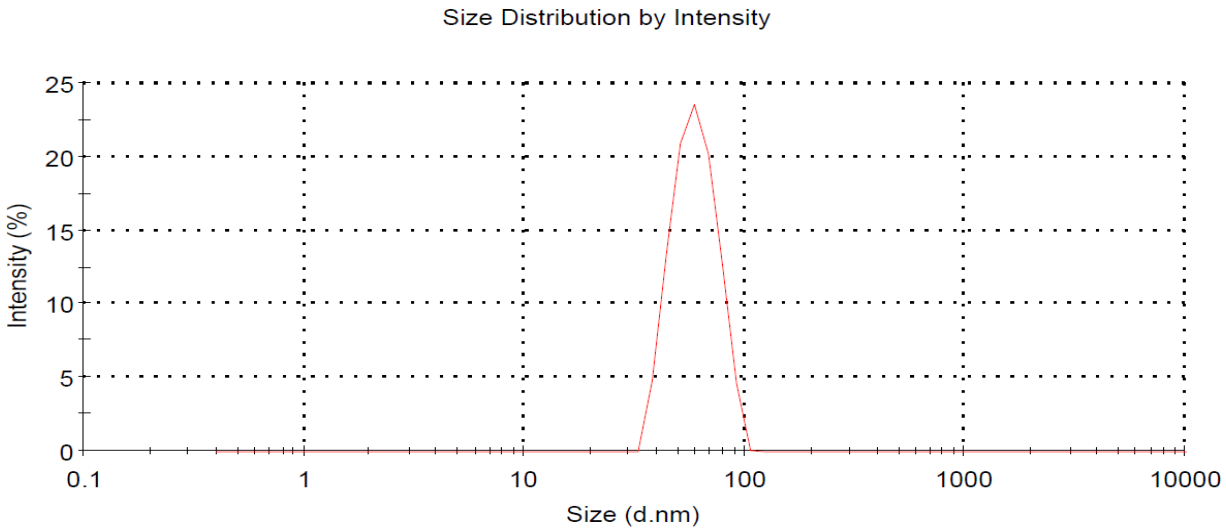

Figure B.1. Size distribution by intensity of 40 nm CM-PSNPs suspended in Nanopure water using Malvern Zetasizer Nano-ZS. Abbreviation: d: diameter.

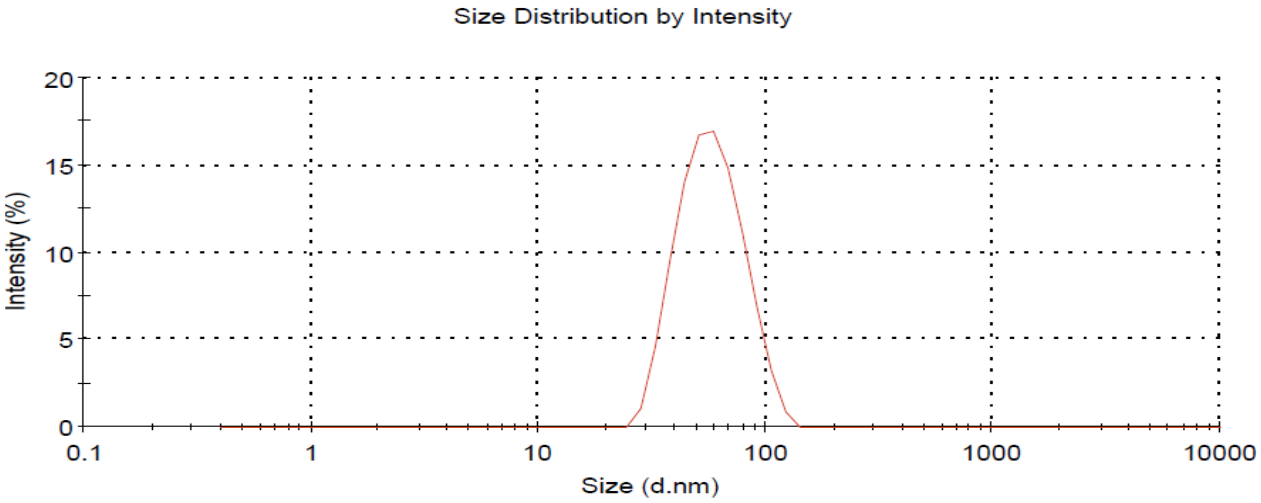

Figure B.2. Size distribution by intensity of 40 nm CM-PSNPs suspended in KRB using Malvern Zetasizer Nano-ZS. Abbreviation: d: diameter

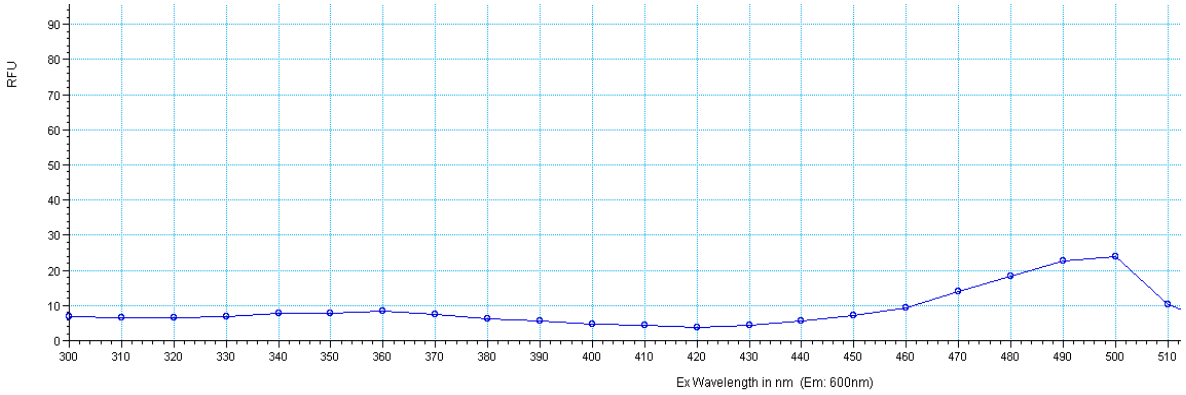

Figure B.3. Excitation spectrum of fluorescein using SpectraMax M5 Multi-Mode Microplate Reader. Abbreviations: RFU: relative fluorescence units, Ex: excitation, Em: emission.

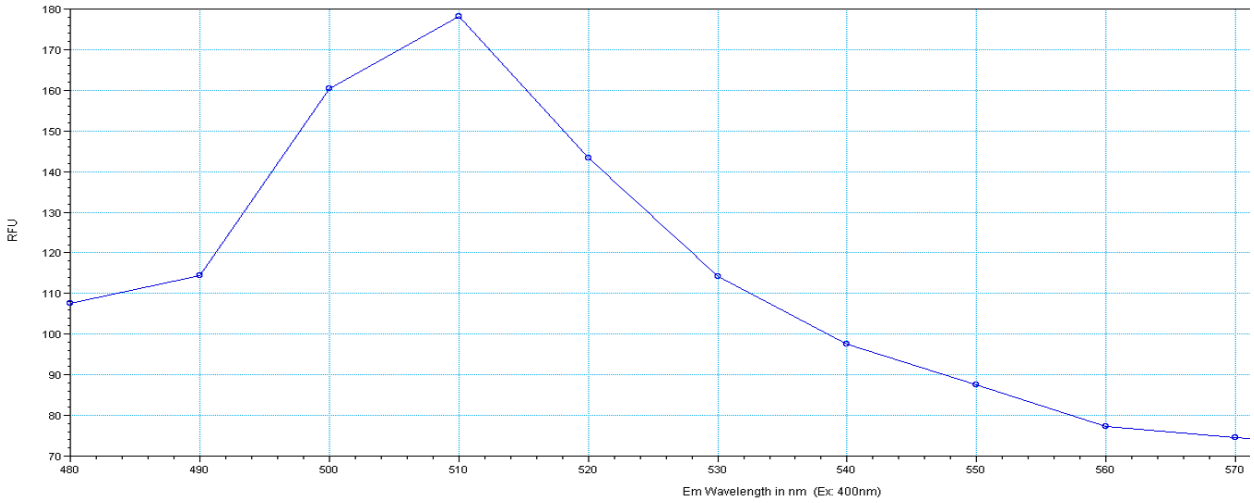

Figure B.4. Emission spectrum of fluorescein using SpectraMax M5 Multi-Mode Microplate Reader. Abbreviations: RFU: relative fluorescence units, Em: emission, Ex: excitation.

APPENDIX C

Example Calculation for Mass of Nanoparticles:

Initial Concentration of Nanoparticles in the Donor Chamber (%) w/v	Initial Volume Donor chamber (mL)	Initial Mass of Nanoparticles in the Donor Chamber (µg)	Mean Mass of Full-thickness Nasal Olfactory Tissue (g) ± SD	Mean Mass of Full-thickness Nasal Respiratory Tissue (g) ± SD	Estimated Mass of Nanoparticles per Gram of Full-thickness Nasal Olfactory Tissue (µg/ g) in the Donor Chamber	Estimated Mass of Nanoparticles per Gram of Full-thickness Nasal Respiratory Tissue (µg/ g) in the Donor Chamber
0.1%	1mL	1000	0.046 ± 0.01	0.071 ± 0.02	21709.6	14058.4

Table C.1. Nanoparticle concentration, mass, and mass/ µg of tissue estimates for initial donor chamber conditions.

Fluorescence readings and mass calculations of 40 nm CM-PSNPs:

Sample	Time (min)	Mean Fluorescence Reading ± SD	Mean Nanoparticle Concentration (µg/ mL) ± SD	Mean Total Nanoparticle Mass (µg) ± SD	Mean Mass of Nanoparticles per Gram of Full-thickness Tissue (µg/ g) ± SD	Total Mass of Nanoparticles per Gram of Full-thickness Tissue (µg/ g) ± SD in the Donor Chamber
Full-thickness	30	12.64 ± 9.33	0.46 ± 0.28	1.38 ± 0.93	34.13 ± 29.5	23794.7 ± 9677.8
	60	17.15 ± 12.5	0.6 ± 0.38	1.8 ± 1.25	45.95 ± 32.83	25346.8 ± 6680
Epithelium	30	21.28 ± 4.12	0.73 ± 0.13	2.19 ± 0.43	54.9 ± 29.18	23794.7 ± 9677.8
	60	29.28 ± 1.16	0.98 ± 0.03	2.95 ± 0.07	75.16 ± 18.82	25346.8 ± 6680
Submucosa	30	3.99 ± 0.32	0.18 ± 0.01	0.56 ± 0.01	13.27 ± 4.39	23794.7 ± 9677.8
	60	5.03 ± 0.19	0.21 ± 0.006	0.65 ± 0.009	16.74 ± 4.05	25346.8 ± 6680.1

Table C.2. Calculations of 40 nm CM-PSNP content of the nasal olfactory mucosa in untreated transport studies, n=3.

sample	Time (min)	Mean Fluorescence Reading ± SD	Mean Nanoparticle Concentration (µg/ mL) ± SD	Mean Total Nanoparticle Mass (µg) ± SD	Mean Mass of Nanoparticles per Gram of Full-thickness Tissue (µg/ g) ± SD	Total Mass of Nanoparticles per Gram of Full-thickness Tissue (µg/ g) ± SD in the Donor Chamber
Full-thickness	30	15.18 ± 11.4	0.53 ± 0.35	1.61 ± 1.14	30.13 ± 20.81	18535 ± 3236
	60	10.13 ± 4.29	0.38 ± 0.13	1.14 ± 0.43	25.96 ± 8.93	22900.4 ± 2290
Epithelium	30	25.52 ± 5.93	0.86 ± 0.18	2.59 ± 0.64	48.85 ± 12.96	18535 ± 3236
	60	14.15 ± 1.62	0.5 ± 0.05	1.52 ± 0.16	34.61 ± 1.017	22900.4 ± 2290
Submucosa	30	4.84 ± 0.64	0.21 ± 0.02	0.64 ± 0.06	11.9 ± 2.2	18535 ± 3236
	60	6.11 ± 0.47	0.25 ± 0.01	0.76 ± 0.01	17.42 ± 2.02	22900.4 ± 2290

Table C.3. Calculations of 40 nm CM-PSNP content of the nasal olfactory mucosa using pharmacologic inhibitor (chlorpromazine) in the transport studies, n=3.

Sample	Time (min)	Mean Fluorescence Reading ± SD	Mean Nanoparticle Concentration (µg/ mL) ± SD	Mean Total Nanoparticle Mass (µg) ± SD	Mean Mass of Nanoparticles per Gram of Full-thickness Tissue (µg/ g) ± SD	Total Mass of Nanoparticles per Gram of Full-thickness Tissue (µg/ g) ± SD in the Donor Chamber
Full-thickness	30	14.14 ± 10.5	0.5 ± 0.33	1.52 ± 1.05	29.45 ± 22.74	19137.7 ± 6243.2
	60	14.91 ± 8.77	0.53 ± 0.27	0.23 ± 0.02	33.5 ± 17.39	21071.6 ± 1024.5
Epithelium	30	24.2 ± 2.47	0.82 ± 0.07	2.47 ± 0.26	50.55 ± 17.57	19137.7 ± 6243.2
	60	23.05 ± 3.4	0.78 ± 0.1	0.25 ± 0.02	50.37 ± 6.53	21071.6 ± 1024.5
Submucosa	30	4.07 ± 0.54	0.19 ± 0.01	0.57 ± 0.05	10.77 ± 2.4	19137.7 ± 6243.2
	60	6.78 ± 1.73	0.27 ± 0.05	0.2 ± 0.005	17.29 ± 2.98	21071.6 ± 1024.5

Table C.4. Calculations of 40 nm CM-PSNP content of the nasal olfactory mucosa using pharmacologic inhibitor (amiloride) in the transport studies, n=3.

Sample	Time (min)	Mean Fluorescence Reading ± SD	Mean Nanoparticle Concentration (µg/ mL) ± SD	Mean Total Nanoparticle Mass (µg) ± SD	Mean Mass of Nanoparticles per Gram of Full-thickness Tissue (µg/ g) ± SD	Total Mass of Nanoparticles per Gram of Full-thickness Tissue (µg/ g) ± SD in the Donor Chamber
Full-thickness	30	7.85 ± 3.57	0.3 ± 0.11	0.92 ± 0.36	22.39 ± 8.72	24164.2 ± 3627.5
	60	12.38 ± 7.53	0.45 ± 0.23	1.35 ± 0.75	38.02 ± 20.7	28054.9 ± 3723.9
Epithelium	30	11.32 ± 0.15	0.41 ± 0.005	1.25 ± 0.0009	30 ± 3.97	24164.2 ± 3627.5
	60	19.7 ± 0.56	0.68 ± 0.1	2.04 ± 0.04	58.04 ± 7.47	28054.9 ± 3723.9
Submucosa	30	4.38 ± 0.21	0.2 ± 0.006	0.6 ± 0.02	14.5 ± 2.3	24164.2 ± 3627.5
	60	5.08 ± 0.37	0.22 ± 0.01	0.66 ± 0.02	18.58 ± 1.99	28054.9 ± 3723.9

Table C.5. Calculations of 40 nm CM-PSNP content of the nasal olfactory mucosa using pharmacologic inhibitor (m-βCD) in the transport studies, n=3.

Sample	Time (min)	Mean Fluorescence Reading ± SD	Mean Nanoparticle Concentration (µg/ mL) ± SD	Mean Total Nanoparticle Mass (µg) ± SD	Mean Mass of Nanoparticles per Gram of Full-thickness Tissue (µg/ g) ± SD	Total Mass of Nanoparticles per Gram of Full-thickness Tissue (µg/ g) ± SD in the Donor Chamber
Full-thickness	30	6.76 ± 2.16	0.27 ± 0.06	0.82 ± 0.21	15.3 ± 3.81	18589.1 ± 609.4
	60	15.35 ± 10.56	0.54 ± 0.33	1.63 ± 1.06	36.7 ± 24.6	22391.8 ± 5800.8
Epithelium	30	8.85 ± 0.012	0.34 ± 0.01	1.02 ± 0.016	18.98 ± 0.69	18589.1 ± 609.4
	60	25.54 ± 1.72	0.86 ± 0.05	2.59 ± 0.17	56.6 ± 14.46	22391.8 ± 5800.8
Submucosa	30	4.68 ± 0.1	0.2 ± 0.003	0.62 ± 0.0003	11.63 ± 0.37	18589.1 ± 609.4
	60	5.16 ± 0.69	0.22 ± 0.02	0.67 ± 0.07	14.9 ± 3.16	22391.8 ± 5800.8

Table C.6. Calculations of 40 nm CM-PSNP content of the nasal respiratory mucosa in untreated transport studies, n=3.

Sample	Time (min)	Mean Fluorescence Reading ± SD	Mean Nanoparticle Concentration (µg/ mL) ± SD	Mean Total Nanoparticle Mass (µg) ± SD	Mean Mass of Nanoparticles per Gram of Full-thickness Tissue (µg/ g) ± SD	Total Mass of Nanoparticles per Gram of Full-thickness Tissue (µg/ g) ± SD in the Donor Chamber
Full-thickness	30	7.92 ± 3.03	0.31 ± 0.09	0.93 ± 0.3	12.28 ± 3.77	13336 ± 2382.7
	60	15.1 ± 8.33	0.53 ± 0.26	1.61 ± 0.83	15.48 ± 5.27	10324.9 ± 2032.2
Epithelium	30	10.71 ± 0.99	0.39 ± 0.03	1.19 ± 0.1	15.93 ± 1.29	13336 ± 2382.7
	60	15.79 ± 9.31	0.55 ± 0.29	1.67 ± 1.01	16.8 ± 5.97	10324.9 ± 2032.2
Submucosa	30	5.13 ± 1.01	0.22 ± 0.03	0.66 ± 0.1	8.78 ± 0.95	13336 ± 2382.7
	60	14.4 ± 7.73	0.51 ± 0.24	1.54 ± 0.83	14.9 ± 4.75	10324.9 ± 2032.2

Table C.7. Calculations of 40 nm CM-PSNP content of the nasal respiratory mucosa using pharmacologic inhibitor (chlorpromazine) in the transport studies, n=3.

Sample	Time (min)	Mean Fluorescence Reading ± SD	Mean Nanoparticle Concentration (µg/ mL) ± SD	Mean Total Nanoparticle Mass (µg) ± SD	Mean Mass of Nanoparticles per Gram of Tissue (µg/ g) ± SD	Total Mass of Nanoparticles per Gram of Full-thickness Tissue (µg/ g) ± SD in the Donor Chamber
Full-thickness	30	8.21 ± 2.49	0.32 ± 0.07	0.96 ± 0.24	11.14 ± 3.65	11546.9 ± 3006.8
	60	17.3 ± 12.57	0.6 ± 0.39	1.82 ± 1.26	27.62 ± 19.21	15074.3 ± 2392.9
Epithelium	30	10.11 ± 2.06	0.38 ± 0.06	1.13 ± 0.22	13.37 ± 3.24	11546.9 ± 3006.8
	60	29.33 ± 3.18	0.98 ± 0.1	2.95 ± 0.33	44.45 ± 10.23	15074.3 ± 2392.9
Submucosa	30	6.31 ± 0.92	0.26 ± 0.03	0.78 ± 0.08	9.15 ± 2.94	11546.9 ± 3006.8
	60	5.27 ± 0.31	0.22 ± 0.009	0.68 ± 0.01	10.26 ± 1.32	15074.3 ± 2392.9

Table C.8. Calculations of 40 nm CM-PSNP content of the nasal respiratory mucosa using pharmacologic inhibitor (amiloride) in the transport studies, n=3.

Sample	Time (min)	Mean Fluorescence Reading ± SD	Mean Nanoparticle Concentration (µg/ mL) ± SD	Mean Total Nanoparticle Mass (µg) ± SD	Mean Mass of Nanoparticles per Gram of Tissue (µg/ g) ± SD	Total Mass of Nanoparticles per Gram of Full-thickness Tissue (µg/ g) ± SD in the Donor Chamber
Full-thickness	30	8.48 ± 2.65	0.32 ± 0.08	0.98 ± 0.26	13.62 ± 4.37	13651 ± 1328.2
	60	14 ± 6.2	0.5 ± 0.19	1.5 ± 0.62	20.5 ± 8.45	13600.3 ± 2212.6
Epithelium	30	10 ± 3.01	0.37 ± 0.09	1.12 ± 0.32	15.54 ± 5.21	13651 ± 1328.2
	60	19.73 ± 2.75	0.68 ± 0.08	2.04 ± 0.29	27.87 ± 5.09	13600.3 ± 2212.6
Submucosa	30	6.95 ± 0.83	0.26 ± 0.03	0.84 ± 0.08	11.55 ± 1.96	13651 ± 1328.2
	60	8.26 ± 0.09	0.32 ± 0.003	0.96 ± 0.009	13.11 ± 1.85	13600.3 ± 2212.6

Table C.9. Calculations of 40 nm CM-PSNP content of the nasal respiratory mucosa using pharmacologic inhibitor (m-βCD) in the transport studies, n=3.

Tissue Type	Time (min)	Mean TEER Values in Non-Inhibited Tissue ± SD		Mean TEER Values in CPZ Treated Tissue ± SD		Mean TEER Values in Amiloride Treated Tissue ± SD		Mean TEER Values in M-βCD Treated Tissue ± SD	
		Starting Time	Ending Time	Starting Time	Ending Time	Starting Time	Ending Time	Starting Time	Ending Time
Nasal Respiratory Tissue	30	156.6 ± 28.5	155.3 ± 30.5	224.3 ± 13.5	216 ± 14.8	201.6 ± 33.3	195.6 ± 34	163.6 ± 6.3	158.6 ± 15.8
	60	190 ± 25	186.3 ± 25	210 ± 38.7	206 ± 35.5	206 ± 21.9	205 ± 25.2	174.6 ± 7.5	168.6 ± 3.2
Nasal Olfactory Tissue	30	126.6 ± 9	125 ± 5.1	200.3 ± 8.5	190.3 ± 5	142.6 ± 8	143 ± 8.7	151 ± 9.6	147.6 ± 6.5
	60	137 ± 30.8	134.6 ± 30.1	222.6 ± 16	215 ± 20.8	125.6 ± 9.4	123 ± 12.5	148 ± 10.4	145.6 ± 7.2

Table C.10. TEER measurements ($\Omega.cm^2$) of the full-thickness nasal respiratory and olfactory mucosa after exposure to different treatments at the 5 min starting time and at the 30 min and 60 min ending time of the transport experiments, n=3.

Sample of calculation:

1- The fluorescence intensity was measured after incubation.

   Ex. The fluorescence reading of epithelium untreated olfactory tissue (30 min transport study period) was found to be 25.

2- The fluorescence reading obtained from step 1 was used in predetermined correlation [Figure 3.1] to find the concentration of the particles.

   Ex. Nanoparticle conc. = (25 + 1.94)/31.72 = 0.849 µg/ mL.

3- The total mass of the particles per gram of full-thickness tissue was obtained by multiplying the concentration of the particles by the total volume of the solvent that was used for extraction and dividing the result by the tissue mass in gram.

   Ex. (0.849 µg/ mL * 3 mL)/ (0.029 g) = 87.9 µg/ g.

4- The total mass of the particles per gram of full-thickness tissues in the donor chamber was obtained by dividing the initially applied mass by the tissue mass in gram.

   Ex. 0.1% = 1000 µg/ mL. Since the initially applied volume is 1mL, then

   1000 µg / (0.029 g) = 34482.7 µg/ g.

REFERENCES

1. Gupta, N., B. Patel, and F. Ahsan, *Pulmonary and Nasal Drug Delivery*, in *Drug Delivery*, A.K. Mitra, D. Kwatra, and A.D. Vadlapudi, Editors. 2015, Jones & Bartlett Publishers. p. 326-327.

2. Bitter, C., K. Suter-Zimmermann, and C. Surber, *Nasal Drug Delivery in Humans*, in *Topical Applications and the Mucosa*, C. Surber, P. Elsner, and M.A. Farage, Editors. 2011, Karger Publishers. p. 20-35.

3. McDonough, J., H. Dixon, and M. Ladika, *Nasal Delivery of Micro- and Nano-encapsulated Drugs*, in *Handbook of Non-Invasive Drug Delivery Systems*, V.S. Kulkarni, Editor. 2009, Elsevier. p. 193-194.

4. Ugwoke, M.I., N. Verbeke, and R. Kinget, *The biopharmaceutical aspects of nasal mucoadhesive drug delivery.* Journal of Pharmacy and Pharmacology, 2001. **53**(1): p. 3-22.

5. Mygind, N. and R. Dahl, *Anatomy, physiology and function of the nasal cavities in health and disease.* Advanced Drug Delivery Reviews, 1998. **29**(1): p. 3-12.

6. Marttin, E., N.G. Schipper, J.C. Verhoef, and F.W. Merkus, *Nasal mucociliary clearance as a factor in nasal drug delivery.* Advanced Drug Delivery Reviews, 1998. **29**(1): p. 13-38.

7. Slomianka, L. *Blue Histology - Respiratory System*. 6/08/09 [cited 2016 22/7]; Available from: http://www.lab.anhb.uwa.edu.au/mb140/CorePages/Respiratory/respir.htm.

8. Mescher, A.L., *The Respiratory System* in *Junqueira's Basic Histology*, A.L. Mescher, Editor. 2005, London: McGraw Hill. p. 343-363.

9. Moran, D.T., J.C. Rowley III, B.W. Jafek, and M.A. Lovell, *The fine structure of the olfactory mucosa in man.* Journal of Neurocytology, 1982. **11**(5): p. 721-746.

10. Suman, J.D., *Current understanding of nasal morphology and physiology as a drug delivery target.* Drug Delivery and Translational Research, 2013. **3**(1): p. 4-15.

11. Grassin-Delyle, S., A. Buenestado, E. Naline, C. Faisy, S. Blouquit-Laye, L.-J. Couderc, M. Le Guen, M. Fischler, and P. Devillier, *Intranasal drug delivery: an efficient and non-invasive route for systemic administration: focus on opioids.* Pharmacology & Therapeutics, 2012. **134**(3): p. 366-379.

12. Gupta, R.B., *Fundamentals of Drug Nanoparticles*, in *Nanoparticle Technology for Drug Delivery*, B.G. Ram and B.K. Uday, Editors. 2006, New York, USA: Taylor & Francis Group Inc. p. 6.

13. Gupta, R.B., *Fundamentals of Drug Nanoparticles*, in *Nanoparticle Technology for Drug Delivery*, B.G. Ram and B.K. Uday, Editors. 2006, New York, USA: Taylor & Francis Group Inc. p. 1-2.

14. Sahay, G., D.Y. Alakhova, and A.V. Kabanov, *Endocytosis of nanomedicines.* Journal of Controlled Release, 2010. **145**(3): p. 182-195.

15. Yameen, B., W.I. Choi, C. Vilos, A. Swami, J. Shi, and O.C. Farokhzad, *Insight into nanoparticle cellular uptake and intracellular targeting.* Journal of Controlled Release, 2014. **190**: p. 485-499.

16. Sirisaengtaksin, N., B.S. Brown, and A.J. Bean, *Endocytosis*, in *Mass Transport of Nanocarriers*, R.E. Serda, Editor. 2012, CRC Press. p. 242.

17. McMahon, H.T. and E. Boucrot, *Molecular mechanism and physiological functions of clathrin-mediated endocytosis.* Nature Reviews Molecular Cell Biology, 2011. **12**(8): p. 517-533.

18. Simons, K. and D. Toomre, *Lipid rafts and signal transduction.* Nature Reviews Molecular Cell Biology, 2000. **1**(1): p. 31-39.

19. Iversen, T.-G., T. Skotland, and K. Sandvig, *Endocytosis and intracellular transport of nanoparticles: present knowledge and need for future studies.* Nano Today, 2011. **6**(2): p. 176-185.

20. Khalil, I.A., K. Kogure, H. Akita, and H. Harashima, *Uptake pathways and subsequent intracellular trafficking in nonviral gene delivery.* Pharmacological Reviews, 2006. **58**(1): p. 32-45.

21. Ivanov, A.I., *Pharmacological Inhibition of Endocytic Pathways: Is It Specific Enough to Be Useful?*, in *Exocytosis and Endocytosis*, A.I. Ivanov, Editor. 2008, Springer. p. 15-28.

22. Wang, L.-H., K.G. Rothberg, and R. Anderson, *Mis-assembly of clathrin lattices on endosomes reveals a regulatory switch for coated pit formation.* The Journal of Cell Biology, 1993. **123**(5): p. 1107-1117.

23. Koivusalo, M., C. Welch, H. Hayashi, C.C. Scott, M. Kim, T. Alexander, N. Touret, K.M. Hahn, and S. Grinstein, *Amiloride inhibits macropinocytosis by lowering submembranous pH and preventing Rac1 and Cdc42 signaling.* The Journal of Cell Biology, 2010. **188**(4): p. 547-563.

24. Smart, E.J. and R.G. Anderson, *[13]-Alterations in Membrane Cholesterol That Affect Structure and Function of Caveolae.* Methods in Enzymology, 2002. **353**: p. 131-139.

25. Westermann, M., F. Steiniger, and W. Richter, *Belt-like localisation of caveolin in deep caveolae and its re-distribution after cholesterol depletion.* Histochemistry and Cell Biology, 2005. **123**(6): p. 613-620.

26. Rodal, S.K., G. Skretting, O. Garred, F. Vilhardt, B. Van Deurs, and K. Sandvig, *Extraction of cholesterol with methyl-β-cyclodextrin perturbs formation of clathrin-coated endocytic vesicles.* Molecular Biology of the Cell, 1999. **10**(4): p. 961-974.

27. Chen, N., *Size and surface properties determining nanoparticle uptake and transport in the nasal mucosa*. 2013, University of Iowa: Iowa City, IA 52242.

28. Invitrogen™. *FluoSpheres ® Fluorescent Microspheres*. 2005 [cited 2016 7/28]; Available from: https://tools.thermofisher.com/content/sfs/manuals/mp05000.pdf.

29. FMRC. *Manual for Using Fluorescent Microspheres to Measure Regional Organ Perfusion*. 2015 [cited 2016 7/28]; Available from: http://fmrc.pulmcc.washington.edu/DOCUMENTS/FMRCMAN.pdf.

30. Probes®, M. *FluoSpheres® Fluorescent Microspheres for Tracer Studies*. 2003 [cited 2016 7/28]; Available from: https://tools.thermofisher.com/content/sfs/manuals/mp13080.pdf.

31. Lang, S., P. Langguth, R. Oschmann, B. Traving, and H.P. Merkle, *Transport and metabolic pathway of thymocartin (TP4) in excised bovine nasal mucosa.* Journal of Pharmacy and Pharmacology, 1996. **48**(11): p. 1190-1196.

32. Schmidt, M.C., D. Simmen, M. Hilbe, P. Boderke, G. Ditzinger, J. Sandow, S. Lang, W. Rubas, and H.P. Merkle, *Validation of excised bovine nasal mucosa as in vitro model to study drug transport and metabolic pathways in nasal epithelium.* Journal of Pharmaceutical Sciences, 2000. **89**(3): p. 396-407.

33. Koch, A.M., M.C. Schmidt, and H.P. Merkle, *In vitro methodologies to study nasal delivery using excised mucosa.* Cell Culture Models of Biological Barriers: In vitro Test Systems for Drug Absorption and Delivery, 2002: p. 228.

34. FMRC. *Standard Curves, Fluorescent Controls, Background Fluorescence & Sources of Error*. 2015 2015-12-31 [cited 2016 7/22]; Available from: http://fmrc.pulmcc.washington.edu/DOCUMENTS/FMRC3.pdf.

35. Gilbert, T.W., T.L. Sellaro, and S.F. Badylak, *Decellularization of tissues and organs.* Biomaterials, 2006. **27**(19): p. 3675-3683.

36. Zhang, L.W. and N.A. Monteiro-Riviere, *Mechanisms of quantum dot nanoparticle cellular uptake.* Toxicological Sciences, 2009. **110**(1): p. 138-155.

37. Rejman, J., V. Oberle, I.S. Zuhorn, and D. Hoekstra, *Size-dependent internalization of particles via the pathways of clathrin-and caveolae-mediated endocytosis.* Biochemical Journal, 2004. **377**(1): p. 159-169.

38. Lai, S.K., K. Hida, S.T. Man, C. Chen, C. Machamer, T.A. Schroer, and J. Hanes, *Privileged delivery of polymer nanoparticles to the perinuclear region of live cells via a non-clathrin, non-degradative pathway.* Biomaterials, 2007. **28**(18): p. 2876-2884.

39. Dos Santos, T., J. Varela, I. Lynch, A. Salvati, and K.A. Dawson, *Effects of transport inhibitors on the cellular uptake of carboxylated polystyrene nanoparticles in different cell lines.* PLoS One, 2011. **6**(9): p. e24438.